ION BEAM ENERGY CALIBRATION OF THE 1.7 MV TANDEM ACCELERATOR AT GAEC

A Thesis submitted to the Department of

NUCLEAR SCIENC E AND APPLICATIONS

COLLEGE OF BASIC AND APPLIED SCIENCES

UNIVERSITY OF GHANA

BY

EDWARD BERCHIE

Bsc (Cape-Coast), 2014

10552046

In partial fulfilment of the requirements for the degree of

MASTER OF PHILOSOPHY

In

APPLIED NUCLEAR PHYSICS

July 2018

DECLARATION

I, MR. EDWARD BERCHIE, hereby declare that with the exception of references to other people's work which have been duly acknowledged, this thesis is the result of my own research work and no part of it has been presented for another degree at this University or elsewhere. I also declare that the preparation of this thesis was supervised in accordance with the guidelines of supervision of thesis work laid down by the University of Ghana.

…… ……

EDWARD BERCHIE Date

(Candidate)

…….. ……

DR. CHRISTIAN NUVIADENU DR. JOSEPH B. TANDOH

(PRINCIPAL SUPERVISOR) (CO-SUPERVISOR)

…… ……

Date Date

DEDICATION

This research work is dedicated to my parents Mr. Martin K. Yeboah, Miss. Juliana Ntoriwaa, Mrs. Christiana Yeboah and to all my siblings for their continued support for my education. May the Lord bless you.

ACKNOWLEDGEMENTS

I wish to express my heartfelt appreciation to my supervisors, Dr. Christian Nuviadenu and Dr. Joseph B. Tandoh for their advice, patience, support and constructive suggestions during the period of this thesis. I also thank Dr. Amos Forson and all the workers of the Accelerator Research Centre of the Ghana Atomic Energy Commission, GAEC for their numerous support during this thesis work.

My sincere gratitude goes to my entire family, Mr Martin K. Yeboah, Madam Juliana Ntoriwaa, Mrs. Christiana Yeboah, Gyimah Owusu Derrick, Selina Obeng Darkoa, Grace Yeboah, Mr. Daniel Boateng Adams and all who contributed to my education.

To conclude, I require showing appreciation to all my associates particularly all members of Champions and Winners Worship Centre Assemblies of God (CWWC, AG), Rev. Ralph Abdullai Adams, Mr. Daniel Boateng, and to all my friends, especially Jerry Ashong, Eric Amesimeku, Nana Yaa Aboagye and Eugenia Baako for their encouragement and support throughout this work.

LIST OF ABBREVIATIONS

ARC	-	Accelerator Research Centre
GAEC	-	Ghana Atomic Energy Commission
PIXE	-	Proton Induced X-Ray Emission
RBS	-	Rutherford Backscattering Spectrometry
NMR	-	Nuclear Magnetic Resonance
RF	-	Radio Frequency
NEC	-	National Electrostatic Corporation
SSB	-	Silicon Surface Barrier Detector
MCA	-	Multi Channel Analyzer
ADC	-	Analogue to Digital Converter
NRA	-	Nuclear Reaction Analysis
ERD	-	Elastic Recoil Detection
HEIS	-	High Energy Ion Scattering Spectrometry
IAEA	-	International Atomic Energy Agency
RBG	-	Background Radiation
IBANDL	-	Ion Beam Analysis Nuclear Data Library
IBA	-	Ion Beam Analysis

TABLE OF CONTENTS

LIST OF TABLES

LIST OF FIGURES

ABSTRACT

Particle accelerators are often used for both ion implantation and ion beam analysis, therefore the accurate and precise knowledge of the energies of the accelerated ions is essential. From the analytical point of view, the energy of the accelerated ion needs to be known with high precision which can only be achieved through calibration. Ghana Atomic Energy Commission hosts a 1.7 MV tandem accelerator, at the Accelerator Research Centre (ARC). This facility uses ion beam techniques such as Proton Induced X-ray Emission (PIXE) and Rutherford Backscattering Spectrometry (RBS) for elemental composition analysis of materials to address issues in health, biological, archaeological, forensic and other areas of science. This study was designed to calibrate the energy of alpha particle which is mainly used for RBS analysis. The main objective of this study is to develop a quick, but effective and efficient method for calibrating the α (He) beam energies produced by the Accelerator Research Centre facility for Rutherford Backscattering Spectrometry. The detector system (Silicon surface barrier detector) for the RBS technique was also calibrated. The method utilized involved the irradiation of four (4) different sample (Au, Si, Cu and Al) targets with a Helium beam of known energy to find the offset in the RBS detector. Americium (^{241}Am) radioactive target with energy 5.486 MeV was utilized to calibrate the surface barrier detector. Lastly Gold target was irradiated with helium beam at five (5) different accelerator terminal voltages to complete the system energy calibration. At the end of the study, an offset parameter of -70.24 was determined in the channel of the detector system. Detector system constant of 962.8 Channels/MeV was determined. All these parameters were used as input parameters to calibrate the whole accelerator system (ion beam energy and detector). The calibration procedure was tested

against the nuclear resonance method of calibration which is currently utilized at the ARC, and it was found to be in good agreement with published $^{27}Al(\alpha, \alpha_o)^{27}Al$ nuclear reaction resonance data

An efficient and effective accelerator ion beam energy calibration technique has been successfully adopted and implemented. Although this method is highly efficient, it is also very simple and cheap. This because only five steps of energy ranges were used during the processes of the ion beam energy calibration as compared to the several runs of energy range used in nuclear resonance technique of ion beam energy calibration at the ARC facility.

CHAPTER ONE

INTRODUCTION

1.1 BACKGROUND TO THE STUDY

A particle accelerator is an equipment which uses electric fields to accelerate charged particles close to the speed of light and uses magnetic fields to put them in a well-defined beam. In other words, particle accelerators are equipment used to accelerate charged particles to higher energies. A particle accelerator mostly consists of three divisions namely;

i. Particles or ions generation source
ii. Accelerating medium for the particles or ions
iii. Scattering chamber.

Basically, particle accelerators are classified into two groups. These are electrostatic and electrodynamic accelerators (Sarah, 2017). Electrostatic accelerators make use of static electric fields to accelerate particles. A typical electrostatic accelerator is the Pelletron accelerator which has its pellet chain operated at a higher velocity to achieve a higher energy. Figure 1.1 illustrates a typical Pelletron accelerator system.

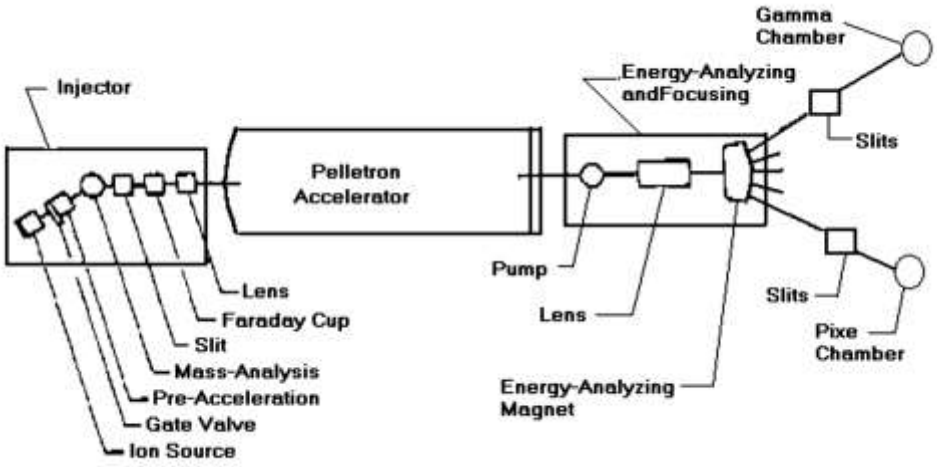

Figure 1. 1: Schematic diagram of a pelletron accelerator system (Barbalat, 1994)

On the other hand, electrodynamic accelerators employ changing electromagnetic fields to accelerate particles. For electrodynamic accelerators, the changing magnetic field is enabled by magnetic induction or oscillating radio frequency fields. This kind of accelerator is either a linear (linac) or a tandem accelerator.

Around the world and in the field of nuclear and atomic physics, particle accelerators are mostly dedicated for qualitative and quantitative analysis of materials. Through the application of particle accelerators, physicists have been able to probe the nucleus and determined its structure and behaviour (Barbalat, 1994).

Particle accelerators are the basic tools for grasping the behaviour of distinct forms of sample materials and the functional and structural behaviour of materials.

Ion beam energies produced by particle accelerators have fast rising applications in nuclear and atomic physics researches as well as in many other areas, such as astrology and

cosmology, medicine and biology, material sciences, environmental studies and the study of art works and archaeological artifacts (Sarah, 2017).

Radiations from ion beam interaction with target materials are characteristics of individual elements present in the materials. In nuclear spectroscopy, distinct ion beam energies are required to cause nuclear reactions so as to identify distinct elements present in a sample during analysis. It is important to perform routine beam energy calibration of particle accelerators so that ion beam energies of the charged ions extracted from them are accurate enough to cause specific nuclear reactions when interacted with the target nuclei.

Ghana's first Accelerator Research Centre (ARC) has been established and was commissioned on the 18th March, 2016. The ARC hosts Ghana's ion beam accelerator, a 1.7 MV Pelletron / Tandem accelerator, at the premise of the Ghana Atomic Energy Commission, (GAEC). According to a technical report released by GAEC (Ghana Atomic Energy, 2015), the function of the ARC in Ghana includes research, application in many areas of the economy and training of human resource in science and technology.

The ARC uses ion beam techniques such as Proton Induced X-ray Emission (PIXE) and Rutherford Backscattering Spectrometry (RBS) for elemental composition analysis of materials. It is also used to address issues in health, biological, archaeological, forensic and other areas of science. This facility requires routine calibrations in order to minimize any measuring uncertainty in results, and also improve quality and accuracy of the ion beam analysis (IBA) technique.

1.1.1 Ion Beam Energy Calibration

In nuclear spectroscopy, specifically at accelerator facilities, ion beam energy calibration is the process of configuring the accelerator system so that the ion beams produced by the accelerator when incident on target materials would cause the required nuclear reactions (www.tempcon.co.uk). A calibrated ion beam of an accelerator system ensures reliable and repeatable measurements in nuclear spectroscopy. Ion Beam energy calibration of a particle accelerator becomes necessary when the accelerator system is restarted after a long period of shutdown. Other factors such as grid misalignment can also cause beam energy loss in accelerator systems. Particle accelerators are required to be calibrated when programs such as modification and improvement are carried out. Such modifications include replacing accelerator components such as the nuclear magnetic resonance (NMR) fluxmeter, coils, and diodes of particle accelerators (Roxana et al., 2012). The main beam types used in the ARC facility are the proton and helium beams.

1.1.2 Ion Beam Calibration Techniques

There are a number of techniques used in calibrating accelerator ion beam energy at any accelerator facility.

Some facilities make use of the resonance and threshold reaction technique. Accelerator calibration using a sufficient number of resonances requires large amount of accelerator beam time since the majority of the resonant nuclear reaction suitable for use in calibration are of low cross-section. Some resonance reactions such as the proton silicon resonance beam energy calibration method have poor precisions (Lane et al, 1993).

There are techniques based on detector technologies such as the time of flight. This technique of ion beam energy calibration is not preferred because it is less precise and requires complex instrumentations even though it takes less accelerator running time (Lane et al, 1993).

Other facilities make use of the magnetic method of ion beam energy calibration (Roxana et al., 2012). This method of ion beam energy calibration is not recommended because it is time consuming, beams of distinct isotopes simultaneously produced can be non-linear if a wide energy range is examined. Also, there is a high probability of analyzing magnet differential hysteresis occurring when the magnetic method of calibrating the ions of an accelerator system is used (Roxana et al., 2012).

Few facilities make use of the non-resonant technique. This method requires independent and expensive calibration of the γ-spectrometer (Calaux et al, 2015). The non-resonant method is time consuming and unsuitable for routine use because the reaction cross-sections of target materials are so low to give accurate and precise ion beam energies (Colaux et al., 2015).

In this work, the RBS energy calibration technique is used. Accelerated ions (α-particles) from the accelerator are elastically scattered from a known target (Au), and the measured energy of the backscattered α-particles are compared to that for the known energy of α-particles from a $10\mu g/cm^2$ thin layer ^{241}Am radioactive source. This method requires neither modification to the experimental setup nor complex instrumentation. Comparing the RBS ion beam energy calibration method being used in this study to the existing resonance method, magnetic method, the non-resonant and time of flight methods, it has

been established that this method is more efficient, accurate, quicker and cost effective (Lane et al, 1993).

1.2 STATEMENT OF RESEARCH PROBLEM

Practically, there could be a difference between the energies of ion beams produced from the tank of the accelerator and what is measured at the detectors; this can be dependent on the many accelerator beam parameters such as the terminal and ion source voltages (Roxana et al., 2012).

At the ARC, the resonance and threshold reaction technique is employed for ion beam energy calibration of accelerated ion beams. However, this technique takes a very long accelerator run time. Also, a wide energy range (1 MeV to 5 MeV) has to be covered at incremental steps of 5 keV per measurement. Consequently, the nuclear resonance and threshold reaction method has become an expensive method of ion beam energy calibration due to the high cost involved in purchasing electricity for an extended accelerator runtime.

1.3 JUSTIFICATION OF STUDY

There are a number of techniques used in calibrating accelerator beam energy at any accelerator facility.

The accelerator facility at GAEC makes use of the resonance and threshold reaction technique to perform energy calibration of the ion beams that it produces. This method of ion beam energy calibration is expensive. It is also associated with a longer accelerator run time because majority of the resonance nuclear reaction suitable for use in beam energy calibration are of low cross-section.

However, the current method being developed would solve the current challenges being faced.

1.4 GENERAL OBJECTIVE OF STUDY

This study seeks to adopt a quick, cost effective but efficient method of ion beam energy calibration as a routine method for the Accelerator Research Centre (ARC) facility at GAEC for reliable ion beam analysis results.

Specific objectives:

This study aims to obtain,

i. a well calibrated detector system with the use of ^{241}Am (americium) radioactive source,
ii. a precisely calibrated accelerator system with the Rutherford Backscattering Spectrometry (RBS) technique.

1.5 ORGANIZATION OF THE REST OF STUDY

The rest of this thesis is organized as follows:

C**hapter two** is the literature review of related matter to the present study. This chapter details the history and development of particle accelerators and the constituents of the accelerator system. This section reveals that the quest for higher energies by the scientific world brought about the idea and the development of particle accelerators. Cockroft-Walton-type multipliers, Van de Graaff generators, Cyclotrons, Synchrotrons, Storage Ring Collider accelerators are discussed in this chapter.

Different kinds of ion sources for particle accelerators have been reviewed in this chapter. Also, the process involved in the production of helium ions, tandem acceleration of helium ions, the PIXE and RBS interaction processes are also discussed in this chapter. Beam diagnostic devices such as the faraday cup, beam transformers, wall current monitors and secondary emission monitors have been discussed. The theory for RBS, where the ion beam (projectile) interacts with target materials has been reviewed.

Chapter 2 also reviews the analyzing endstation system of the accelerator facility. The endstation system reviewed are the vacuum system, the detection system, the computer system and the manipulator system.

Chapter 2 ends by reviewing the various techniques of accelerator ion beam energy calibration. The techniques reviewed are the nuclear resonance and reaction threshold techniques, the magnetic method of ion beam energy calibration and the emerging techniques of ion beam energy calibration with the RBS method found to top the various methods.

C**hapter three** elaborates on the irradiation of the sample materials (gold, silicon, aluminum, copper and glass) and the spectrum collection of the samples using the RC43 data analytical software. The RBS method utilized to facilitate the detector system calibration (the detector offset (C_0) and the detector system constant (β)) and the accelerator system calibration (the voltmeter (V_o) offset and the voltmeter constant (α)) are sequentially discussed in this chapter.

The results and discussions of the RC43 generated spectra of the target samples, the detector system calibration and the entire accelerator system calibration are placed in

chapter four. The validation of the results of this study based on the International Atomic Energy Agency (IAEA) IBANDL database are placed in **chapter four.**

Chapter five concludes the study. This section explains why the RBS method of ion beam energy calibration is chosen for this study, based on simplicity, efficiency and cost effectiveness. This section also provides some recommendations for further study.

CHAPTER 2

LITERATURE REVIEW

2.1 CHAPTER OVERVIEW

This chapter presents a brief overview of the history of development of particle accelerators. The accelerator system comprising ion sources, helium ion production, tandem acceleration of ions, ion beam steering and the scattering chamber are reviewed in this chapter. Also, ion beam diagnostics and the end-station of the accelerator system are discussed. The theory and principle of RBS are also discussed in this chapter. An extensive literature review of some notable methods used for beam energy calibrations of accelerators is carried out here. The chapter ends with a discussion on the emerging techniques for beam energy calibration of accelerator devices.

2.2 HISTORY OF PARTICLE ACCELERATORS

High-energy physics research has always been the reason behind the improvement of particle accelerators.

Beginning with Ernest Rutherford's discovery of a reaction between a nitrogen nucleus and an alpha particle, all research in nuclear physics until 1932 were conducted with alpha particles emitted by the decay of natural radioactive elements (Bryant, 1994). Natural alpha particles have kinetic energies as high as 8 MeV, but Rutherford believed that, in order to observe the disintegration of heavier nuclei by alpha particles, it would be necessary to accelerate alpha particle ions artificially to even higher energies. At the time, it seemed impossible to generate laboratory voltages to accelerate ions to higher energies. Before

then, a calculation by George Gamow proved that considerably less-energetic ions could be useful in some fields but not useful in the nuclear field which requires higher energies to accelerate particles (Gurney, 1928). This result enhanced quests to build an accelerator that could produce a beam of particles needed for nuclear research.

Other advancements of that period brought to light principles still employed in the design of particle accelerators. John Douglas Cockroft and Ernest Thomas Sinton Walton of the University of Cambridge, England conducted the earliest successful experiments with artificially accelerated ions (Walton, 1932). They conducted this experiment by accelerating protons to energies as high as 710 keV, by using a voltage multiplier. The result showed that the accelerated ions reacted with the lithium nucleus to produce two energetic alpha particles (Glass et al., 2014).

At the Princeton University in New Jersey, Robert J. Van de Graaff constructed the first belt-charged electrostatic high-voltage generator. Both the Cockcroft-Walton-type voltage multipliers and Van de Graaff generators are still being used as power sources for accelerators (Van De Graaff, 1931).

Rolf Wideröe, demonstrated the principle of the linear resonance accelerator. Wideröe used alternating high voltage to accelerate ions of sodium and potassium to energies twice as high as those imparted by one application of the peak voltage (Wideröe, 1928).

Ernest O. Lawrence and his assistant in research, David H. Sloan, at the University of California, Berkeley, USA used high-frequency fields to accelerate mercury ions to more than 1.2 MeV. This work strengthened Wideröe's work result in accelerating heavy ions. However, these ion beams produced were not useful in nuclear research because the energy

of the ion beams produced were too less to accelerate particles or interact with target elements.

The cyclotron also called the magnetic resonance accelerator, was envisaged by Lawrence as a correction to the Wideröe's linear resonance accelerator. However, M.S. Livingston, Lawrence's student demonstrated the principle and thus producing 80keV ions. Later, Lawrence and Livingston promulgated the acceleration of protons to more than 1 MeV. The cyclotron energies had reached about 25 MeV and Van de Graaff generators about 4 MeV (Livingston, 1932). Donald W. Kerst, of the University of Illinois built the first betatron (magnetic-induction accelerator of electrons). He built the betatron in the 1940 by utilizing the outcome of orbit calculations to the design of magnets.

After the World War II there was a rapid progress in the science of accelerating particles to high energies. This advancement was started by Edwin Mattison McMillan at Berkeley and Vladimir Iosifovich Veksler at Moscow. Both scientists separately detailed the principle of phase stability. This concept explained a means of sustaining stable particle orbits in the cyclic accelerator. This concept expunged an apparent drawback on the energy of resonance accelerators for protons and made possible the construction of magnetic resonance accelerators called synchrotrons for electrons (McMillan, 1945). Phase focusing, the implementation of the principle of phase stability, was swiftly determined by the construction of a small synchrocyclotron at the University of California and an electron synchrotron in England. Subsequently, the first proton linear resonance accelerator was constructed. All the large proton synchrotrons that have been built depend on this principle.

William W. Hansen, at Stanford University in California, constructed the first traveling-wave linear accelerator of electrons, by making use of the microwave technology that had been developed for radar during World War II (Bryant, 1994).

The advancements in research made possible by increasing the energies of protons led to the building of successively larger accelerators. This trend was ended because of the high cost of fabricating the huge magnet rings with the largest weighing approximately 40,000 tons. A means of increasing the energy without increasing the scale of the machines was provided in a presentation by Livingston, Ernest D. Courant, and H.S. Snyder of the technique of alternating-gradient focusing (sometimes called strong focusing) (Courant, 1952). Synchrotrons incorporating this principle needed magnets only $^{1}/_{100}$ the size that would be required otherwise. All recently constructed synchrotrons make use of alternating-gradient focusing.

Kerst envisioned that, if two sets of particles could be sustained in intersecting orbits, it should be possible to observe interactions in which one particle collided with another moving in the opposite direction. Therefore, the application of this idea requires the build-up of accelerated particles in loops called storage rings (Kerst, 1941). The highest reaction energies that can be obtained have been produced by the use of this technique. Therefore the accelerator produced to create beam energies of such higher energies are the Storage Ring Collider Accelerators (Bryant, 1994).

2.3 THE ACCELERATOR SYSTEM

This accelerator has four main regions namely, ion production also known as the low-energy end of the accelerator system, the region for tandem acceleration of ions, the region for ions focusing and steering and the scattering chamber.

2.3.1 Ion sources

An ion source is a device that produces a beam of ions. Ion sources are used in a number of fields and applications such as mass separation, ion implantation, fusion, space propulsion, atomic physics and in particle accelerators for nuclear and particle physics (Rahman, 2012).

Every ion source consists of two components namely; the plasma generator and the ion extraction system. The extraction system consists of two to four electrodes. Appreciable number of slits are drilled and are properly aligned on the surface of each electrode. The originating electrode is positioned at the same potential as the plasma in the discharge chamber whiles the last electrode is placed at the ground potential.

Figure 2.1 shows a schematic of a two-electrode extraction system

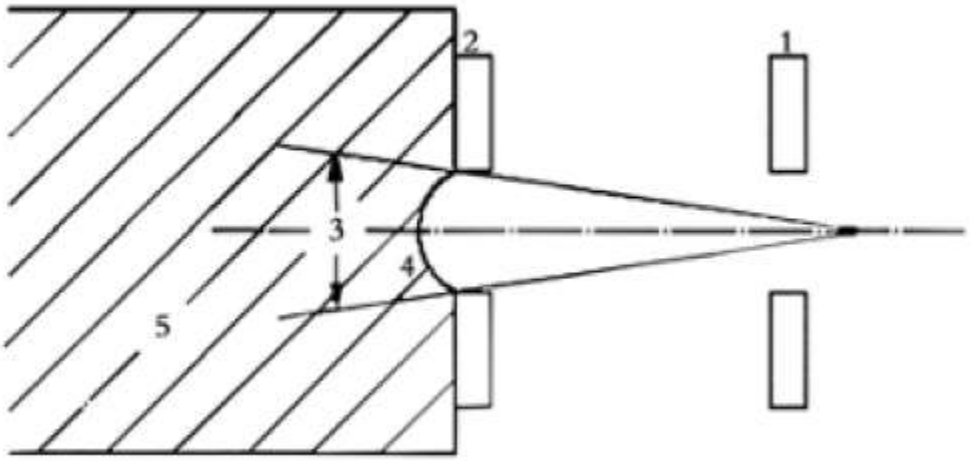

Figure 2. 1: Schematic diagram of a dipole extraction system (the shaded part is the plasma). (1) Ground electrode, (2) extraction electrode, (3) effective angle, (4) plasma boundary, and (5) discharge chamber (Rahman, 2012).

To create a multi-extraction electrode system, a second or third electrode are positioned between the two electrodes. All the electrodes are biased to the required potential, whereas the ions in the plasma at the boundary of the discharge chamber are accelerated to produce an ion beam. The extraction produces an ion beam with a better divergence. Under Optimal conditions, a good extractor produces an ion beam with divergence less than 0.5^{o}.

Ion sources are classified into two main kinds namely; solid surface ion sources and gas/ vapor source. Over the years many different types of ion sources have been produced. These include radio-frequency (RF) sources, radioactive ion sources, duoplasmatron, electron cyclotron resonance sources, the sputter ion source, and many more (Pollock, 2015).

2.3.1.1 Duoplasmatron ion source

Based on the positioning of the intermediate electrode, duoplasmatron ion source can generate a positive or a negative ion. This ion source works on the principle such that a low-pressure arc is created between a cathode and an anode. The cathode filament emits electrons into a vacuum chamber containing a gas. The gas then becomes ionized through interactions with the free electrons from the cathode and subsequently creates a plasma. A dense plasma is then produced in the region of the extraction aperture through a mechanical and magnetic constriction processes. By applying a highly negative or positive potential to the extractor causes the plasma to penetrate through the anode aperture. This process therefore emits positive (proton) ion beam or negative ion beam. Figure 2.2 is a typical diagram of a duoplasmatron ion source.

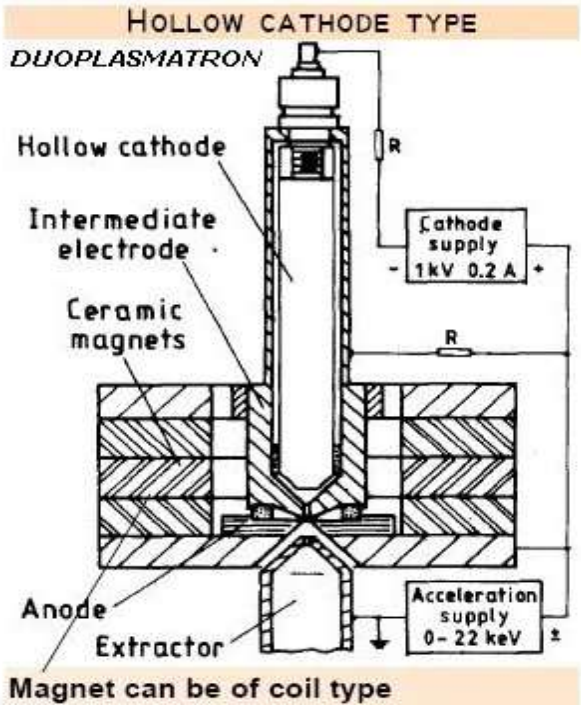

Figure 2. 2: Diagram of the Duoplasmatron ion source (Rahman, 2012)

2.3.1.2 RF Ion Source

With this kind of ion source, plasma of ions is created by the joining of a 100 MHz radio-frequency power to a gas with a pressure of 10^{-3} to 10^{-2} torr. The gas is stored in a container made of glass, quartz or ceramic. Also, the RF is joined to the discharge either through a coil or through two electrodes placed outside the envelope. Relative to the outlet, the plasma is biased whiles the ions extracted via a narrow conduit. Figure 2.3 shows a schematic diagram of an RF ion source.

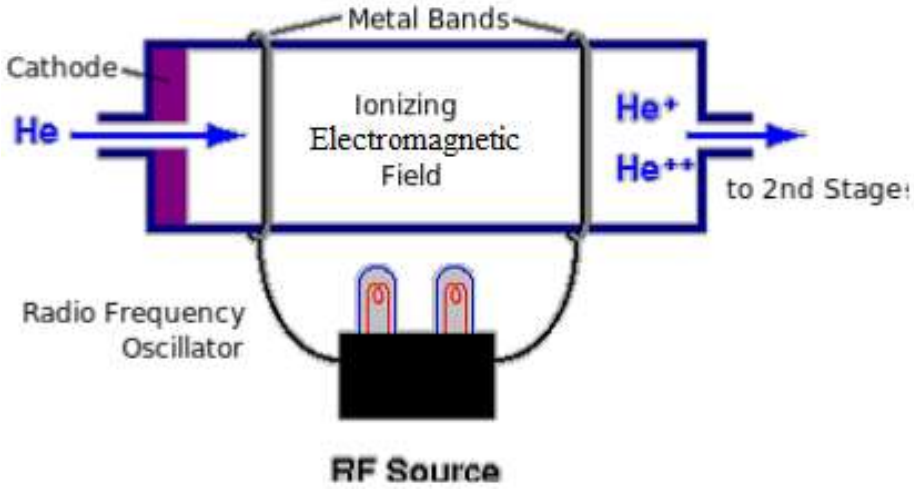

Figure 2. 3: Schematic diagram of an RF ion source (Pollock, 2015)

For the accelerator facility at GAEC, the RF ion source is used for ion beam analysis. The facility together with its associated components were produced by the National Electrostatic Corporation (NEC). The NEC RF-charge exchange ion source, also known to be the Alphatross source, is designed purposely for the production of He^- beams for injection into tandem accelerators. However, this ion source can also produce many other ion beams (Pollock, 2015).

2.3.1.3 He^- ion production

To produce plasma, the gas inlet is fed with He_2. The quartz bottle produces He^+ and other ions after a 100 MHz Radio Frequency (RF) energy is pushed into it. The ions produced are then accelerated into the charge exchanger by applying a potential difference of 6 kV. The helium (He^+) charges produced then passes through a Rubidium (Rb) vapor. Through series of collisions, the helium ion (He^+) picks up an extra negative charge unto itself. He^- charges and other ions are produced through this process. The beam of negative ions produced is then directed to a crossed field (magnetic and electric) analyzer, which selects ions with a well-specified charge (q)/ mass (m) ratio. This crossed-field analyzer has a faraday cup which is meant to count the number of charges produced. The faraday cup also determines the current and intensity of the beam (www.pelletron.com). The He^- charges produced continue on into the accelerator**.** Figure 2.4 illustrates the processes for ion production and acceleration.

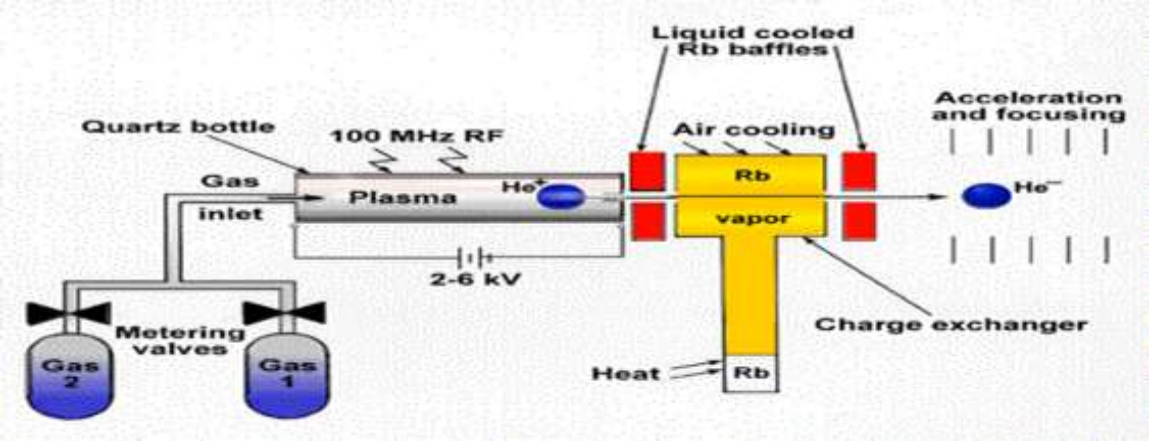

Figure 2. 4: Diagrammatic representation of ion production and acceleration of charge particles in accelerator system (www.pelletron.com)

2.3.2 The tandem or double-staged acceleration of Helium ions.

The He^- ions produced are accelerated toward the middle of the accelerator tank by a 1.7 MV potential difference. With respect to the charge exchanger, the middle of the tank is positive potential for the Pelletron accelerator.

The 1.7 MV potential difference is built by the Pelletron Charging system. Metal pellets and insulating connectors are the constituents of the charging unit. In this system, a chain consisting of metal connectors (links) with nylon separators enhances ways of establishing the accelerating potential as shown in figure 2.5.

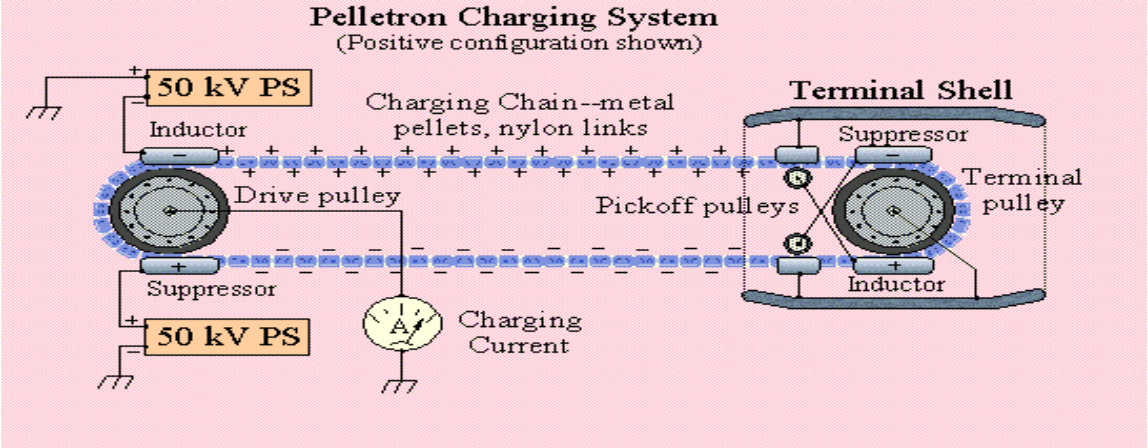

Figure 2. 5: The charging system of a pelletron accelerator (Source: Pelletron Accelerator Charging System; http://www.pelletron.com/charging.htm)

Electrons are pushed off the links to the grounded drive pulley by means of a 50 kV power supply. The power supply charges an inductor within the system. Afterwards, the links are charged positively. The positively charged links then travel to the terminal shell. Also, by obeying Gauss law, electrons from the terminal shell move to the connectors. Through this,

a net positive charge is left on the terminal shell. The terminal shell is positioned near the middle of the accelerator tank (Kelly, 2000).

Before the He^- ions enter the terminal of the accelerator system, they pass through nitrogen gas, which strips them of their electrons producing positive ions, He^+. Since the ions are now positive and are at a positive potential, the charge is accelerated away from the terminal back down 1.7 MV. This acceleration is directed towards the left edge of the terminal. This process produces tandem acceleration of helium ions (www.pelletron.com).

The final energy, E of the emerging positive ions with charge state q is given by equation 2.1:

$$E = V_n + (q+1)V_T \quad [\text{In MeV}] \quad \text{(Kelly, 2000)} \qquad (2.1)$$

($V_n \approx 30$ keV) is the energy of the injected negative ions and V_T being the terminal voltage.

2.3.3 Steering of the Helium ions

The helium ions produced travel away from the accelerator tube through a magnetic quadrupole lens. The lens now focuses the beam produced to a very minute diameter; that is 1cm or less in diameter. The helium ions then enter the beam energy analyzing magnet which then directs them into the various beam lines for use in experimentation (Kelly, 2000).

The beam energy-analyzing magnet of an accelerator system works on the principle of bending path of charged helium ions through the field of the magnetic. The kinetic energy of a moving charged ion or particle is given as:

$$E_P = \frac{mv^2}{2} \quad \text{(Kelly, 2000)} \tag{2.2}$$

The variables, represents the mass of the ions and v indicates the velocity of the ion.

As the charged ions traverses through the field of the magnet, it encounters a magnetic force (F_b). The direction of travel of the charged ions changes.

$$F_b = qvB \tag{2.3}$$

This change in direction of the charged ion generates a centripetal force (F_c),

$$F_C = \frac{mv^2}{r} \tag{2.4}$$

By equating the magnetic and the centripetal forces, the expression below is obtained:

$$qvB = \frac{mv^2}{r} \tag{2.5}$$

Solving equation (2.2) and (2.5), the energy of the ion or particle is determined as:

$$E_P = \frac{(qrB)^2}{2m} \tag{2.6}$$

E_p is the energy of ion or the particle, q is the charge on the ion, m is the mass of the particle, B is the magnetic field strength, and r is the radius by which the trajectory of the ion is bent.

2.3.4 The scattering chambers

This is the experimental confinement vessel or vacuum chamber in which the Rutherford Backscattering Spectrometry (RBS) and Proton Induced X-ray Emission (PIXE**)** experiments are carried out. As the helium ions move into the beam line which is also fixed to the target chamber. The particles with proper orbit or trajectory moves into center of the beam line. The ions with good trajectory are resolved by their kinetic energies, charge-to-mass ratio, and the magnetic field. The alpha particles pass through a vertical slit consisting of two horizontal insulated jaws before entering the target chamber (www.pelletron.com).

Respectively, ions with higher or less energy goes to the inner or outer edges of the beam line. Through this event, the ions encounter the slit jaws. The slit jaws have the function of controlling the beam energy spread with respect to the slit opening. The ions move to the reaction chamber where they interact with target samples under analysis (Kelly, 2000).

2.4 BEAM DIAGNOSTICS

Beam diagnostics refers to the devices meant for acquiring information on the state of the beam and on the advancement and outcome of experiments performed on the beam. Beam diagnostics is an important component of every accelerator (Koziol, 1992). Beam diagnostic helps one to know properties of ion beams and their behavior in the accelerator system. Beam diagnostics monitors analytic beam parameters like emittance, current, size and energy. Some of the diagnostic equipment essential for monitoring and analyzing beam experiments are beam transformers, wall current monitors, faraday cup, secondary emission monitors, beam loss monitors, etc.

There are different significant physical effects that can be used for beam diagnostics. Most of the devices are based on the following physical interactions:

- Electro-magnetic influence:

  The moving charged particles induce electro-magnetic fields around themselves. With appropriate electrodes placed in the close proximity of the beam, these fields are detected and the data relevant to the accelerated particle beam are extracted. Examples are capacitive pick-ups and beam transformers (Goldberg and Lambertson, 1992).

- Coulombic interaction of charged particles and the target material:

  The energy loss of the charged ions in the Coulomb-field of the atoms in the target material results in producing various secondary products such as secondary electrons, positive ions, flourescent light and Brehmstrahlung photons. They can be detected by appropriate devices and can provide data from the interacting particle beam. Examples are beam viewers, secondary emission grids and residual gas monitors (Camas et al, 1993).

- Emission of photons by accelerated particles:

  This kind of diagnostics can only be applied for relativistic particles, i.e. mainly for electron beams or very high-energy proton beams. The emitted photons are in the visible range to the X-ray region of the electromagnetic spectrum. Optical methods can be used; examples are synchrotron radiation monitors (Camas et al, 1993).

- Nuclear- or elementary particle physics interaction:

The beam quantity is determined from the known cross-section and the measured reaction products. Mainly particle detectors are used. Examples are polarimeters or luminosity measurements (Goldberg, 1992).

From Table 2.1, various diagnostic equipment and their parameters are presented.

Table 2. 1: Beam parameters and typical diagnostic equipment

Measured beam parameter	**Diagnostic equipment**
	Faraday-cup
	RF-transformer
Intensity (beam current):	Scintillators
	Ionization chamber
	Secondary electron monitor
Transverse parameters:	
Beam spot (cross-section)	Beam viewers
	Secondary-emission grid
	Wire scanner
Beam profile	Residual gas monitor
	Residual gas fluorescence monitor
	Synchrotron light monitor
Beam position monitor	Capacitive pick-up
	Slit and grid
Transverse emittance	Pepper-pot
	Calculation from beam envelopes
Longitudinal parameters:	
Bunch length, beam phase	Capacitive probe
	Wall-current monitor
Beam energy	Time-of-flight method
	Magnetic analyzer

The selection of a specific device is based on additional factors, which are determined by the type of the accelerator, the characteristics of the particle beam to be measured, the requirements and cost-efficiency of the measurement. Basically, the beam measuring parameters are grouped under three broad parameters. These are intensity parameters, transverse parameters and longitudinal parameters (Koziol, 1992).

2.4.1 Intensity measurement

This is the most basic diagnostic measurement for all accelerators. The number of accelerated particles has to be known not only for the experiments using the beam, but it is a fundamental data for the operation of the machine as well (Goldberg, 1992). The accelerator and beam transport line settings cannot be optimized without being able to measure the end product of the system, i.e. the quantity of the successfully accelerated and transported particles. Since the accelerated particle beams consist of moving electric charges (qe), the determination of their quantity (N) means measuring the current (I) expressed as:

$$I_{beam} = \frac{qeN}{t} = \frac{qeN}{l}\beta c \qquad (2.7)$$

The Faraday-cup being one of the intensity measuring devices is discussed:

2.4.1.1 Faraday cup

Capturing beams with the ordinary collector plate experiences perturbation through secondary electron emission. The diagnostic equipment that prevents this from happening is the use of the faraday cup. Historically, the faraday cup is the first intensity-measuring device produced.

The working principle for the faraday cup is very simple. The beam particles are captured by a piece of isolated conducting material and the excess charge flows from this electrode to the ground through an amperemeter. Figure 2.6 represents a simple Faraday cup.

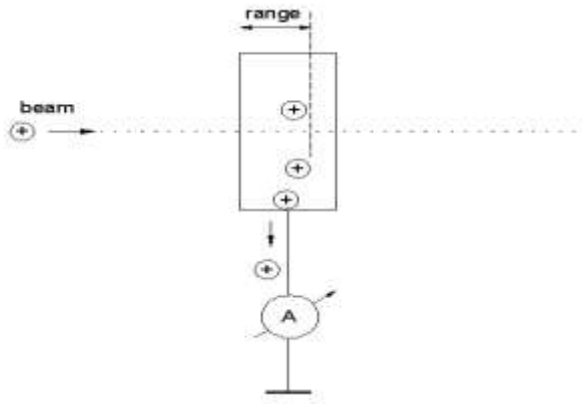

Figure 2. 6: Schematic of a simple Faraday cup.

It is obvious that this method can only be used when the beam particles are captured completely by the electrode. It requires the electrode thickness being greater than the stopping range of the particles in the used electrode material. Since the stopping range increases with beam energy, this type of current measurement is well suited for rather low-energy accelerators.

2.4.1.2 Radio Frequency (RF) Transformer

Signal current goes through the primary winding of the RF transformer. This signal generates a magnetic field that induces a voltage across the secondary winding. Connecting a load to the secondary causes an AC current to flow in the load. RF transformers are widely used in diagnostic equipment for impedance matching to achieve maximum power transfer and to suppress undesired signal reflection, voltage-current step-up or step-down.

2.4.1.3 Scintillators

A scintillator used as a diagnostic consists of a scintillating material, often joined to a light guide, and a photo detector. The scintillating material converts γ- and particle-radiation into light (visible, UV, sometimes X-rays). Mostly, a wavelength shifter is mixed to the primary scintillator. The light guide directs the light to the photo detector. Again a wavelength shifter is often used to match the wave length to the response characteristics of the photo cathode and hence improves the signal. The photo detector converts the light into an electric signal.

2.4.1.4 Ionization chamber

Ionization chamber is a gas-filled, thin-walled chamber with a collector electrode inside. Particles traversing through it will ionize the gas, the ions will travel towards the cathode, the electrons towards the anode and a current can be measured. It is expected that the voltage should be in the "plateau" region where all charges are collected but no avalanche occurs.

2.4.2 Transverse parameters

In most cases we need more information about the accelerated beam than just its quantity. Precise knowledge of the transverse size and position of the beam in the accelerator and the beam transport lines plays a crucial role in optimizing the machine set-up, minimizing beam losses and delivering beams to the experimental apparatus with parameters that are requested by the users (Koziol, 1992). Beam viewers are one of the equipment used to measure the transverse parameters of particle beams.

2.4.2.1 Beam viewers

The simplest way of observing the beam produced is by recording the light emitted from a scintillation screen by the beam. Historically, beam viewers were the first devices that delivered spatial information about the particle beams. Although there is a great number of advanced and more sophisticated beam monitors nowadays, scintillator screens are still in use because of their simplicity, cost effectiveness and power of conviction. Figure 2.7 shows the experimental arrangement for measuring the position of beams and the size of the beam using a scintillator

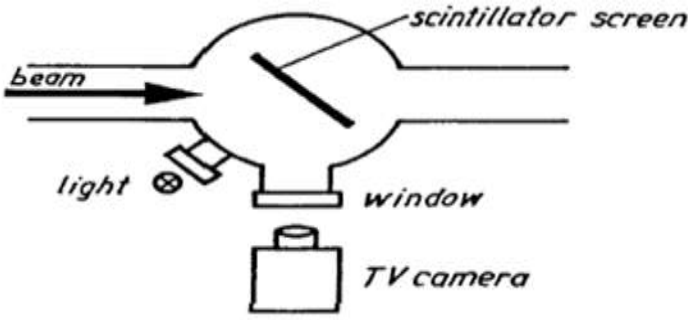

Figure 2. 7: Typical arrangement for observation of beam position and size with a scintillator screen and a TV camera (Goldberg, 1992)

At an angle of 45^{o}, the scintillator screen is placed into the way of the beam. The scintillator bears a graticule which is illuminated through a narrow window in the tank. A TV camera is placed at 90° to the beam direction to observe the 2-dimensional image of the beam cross-section.

2.4.2.2 Secondary- emission grid (SEM)

SEM is a form of an array of thin ribbons used to measure transverse density distribution. Sequential display of the signals from the ribbons gives the beam profile. To enhance the signal strength, either the individual ribbons or the whole array are inclined with respect to the beam direction, thus presenting a greater effective surface. When signal strength is not a problem, the array and the clearing electrodes may be made of thin wires. This makes it a nearly non-destructive profile monitor

2.4.2.3 Wire scanner

Wire scanner as a diagnostic equipment is an electro-mechanical equipment that measures the transverse beam density profile in a particle accelerator by means of a moving thin wire. As the wire passes through the beam, the interaction generates a cascade of secondary particles. These are intercepted by a scintillator, coupled with a photomultiplier, which measures the intensity of the light produced. Also, if a conducting wire material is used, the secondary emission electrons created can also be used to measure the beam profile through the current flow generated on the wire.

2.4.2.4 Residual gas monitor

A residual gas monitor is a small diagnostic device designed for process control and contamination monitoring in vacuum systems. Residual gas monitors are also used as sensitive in-situ leak detectors. They mostly use helium, isopropyl alcohol or other tracer molecules. The vacuum systems are pumped down to lower than 10^{-5} Torr, thereby checking the integrity of the vacuum seals and the quality of the vacuum

2.4.2.5 Capacitive pick-up

Capacitive pick-up is a diagnostic device that converts angular displacement into electrical signal. It consists of ganged capacitance and is based on the principle of variation of effective area of conductors, when other parameters such as separation, distance and dielectric strength being kept constant.

2.4.3 Longitudinal parameters

Besides the two transverse phase spaces there is a third one defined in longitudinal direction. Its coordinates are the momentum spread and the phase deviation. Both coordinates have to be measured with respect of a fictitious reference particle (Koziol, 1992). Due to the proportionality between momentum and energy, using the relative energy spread instead of absolute momentum spread has proven to be very practical. To detect the exact time structure of a particle, beam special diagnostic devices such as the magnetic analyzer is required**.**

2.4.3.1 Beam energy measurement with a magnetic analyzer

When moving in a magnetic field, charged particles experience the Lorentz-force, given by the formula:

$$\overline{F} = qe\bar{v} \times \overline{B} \tag{2.8}$$

$\bar{F} = Lorentz\ force, \qquad q = charge\ of\ the\ particle,$

$e\bar{v} = energy\ of\ the\ particles\ with\ velocity\ \bar{V}$

$\bar{B} = the\ magnetic\ field\ strength$

This magnetic force, being always perpendicular to the velocity of the particles, moves the particles on circular paths. Beside the particle charge and the magnetic field strength, the radius of the circular orbit depends on the particle momentum as well:

$$r = \frac{p}{qeB} \tag{2.9}$$

$r = radius\ of\ orbit, \qquad p = momentum\ of\ the\ particle,$

$q = charge\ of\ the\ particle, \qquad e = electronic\ charge\ and$

$B = the\ magnetic\ field\ strength$

As a consequence, particles with different momentum values move on orbits with different radii in any magnetic field. This dispersive characteristic of the magnetic field can be used to separate particles of different energies and with proper geometry and magnetic field formation one can measure the kinetic energy of the particle beam with high precision (Camas et al, 1993).

Though any bending magnet, which is used to deflect the beam to a required direction, has the dispersion effect, the precision of such a device is usually not enough for beam energy measurements (Koziol, 1992). Special consideration has to be given to the geometry of the system and the applied magnetic field. The geometry has to provide that the beam is deflected by the magnetic field on an exactly defined bending radius. The formation of the magnetic field has to result in precisely known field values all along the bending paths, mostly achieved by forming a highly homogenous magnetic field in the entire region. If only both conditions, which is exact knowledge of the orbit radius and magnetic field strength are fulfilled, it is possible to determine the momentum and energy of the beam with high precision. Such a system is usually called a magnetic analyzer. It is built around a special bending magnet with a rather big deflection angle. A scheme of a magnetic analyzer is shown in figure 2.8 above.

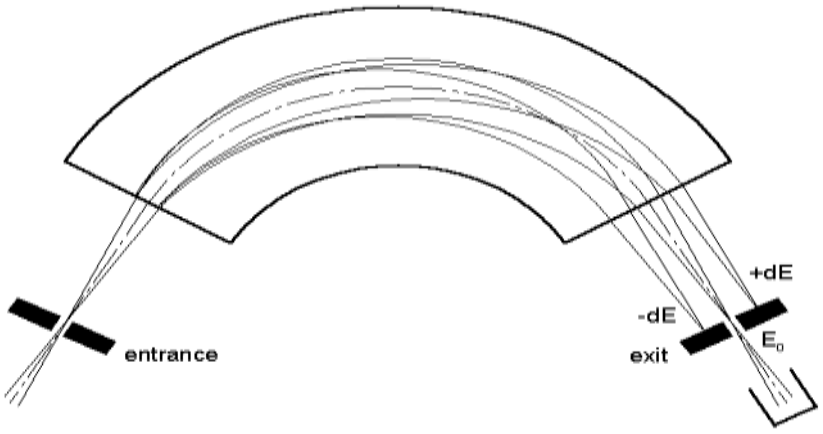

Figure 2. 8: Scheme of a magnetic analyzer (Goldberg, 1992)

In a typical arrangement the two slits, the magnet and the field-free regions between them form an optical system in the deflection plane, where the exit slit is the optical image of

the entrance one. Any particle entering the system through the entrance slit will leave it through the exit slit if its energy value is in accordance with the applied magnetic field (Goldberg, 1992). Detecting the beam behind the exit slit by a current measuring device such as the Faraday-cup, one can calculate the energy value from the known bending radius and the applied magnetic inductance value.

2.5 THEORY OF RUTHERFORD BACKSCATTERING SPECTROMETRY (RBS)

This technique is also called the High-Energy Ion Scattering (HEIS) Spectrometry. RBS helps in the determination of the structure and composition of materials by measuring the backscattering of a beam of high energy ions (typically protons or alpha particles) impinging on a sample.

Rutherford backscattering is an elastic collision between a high kinetic energy particle from the incident beam (the projectile) and a stationary particle located in the sample (the target). It is elastic because no energy is transferred between the incident particle and the stationary particle during the collision, and the state of the stationary particle is unchanged (Oura; Lifshits; Saranin and Zotov, 2003). Figure 2.9 below illustrates the process of RBS; incident helium particles backscattered after incidence.

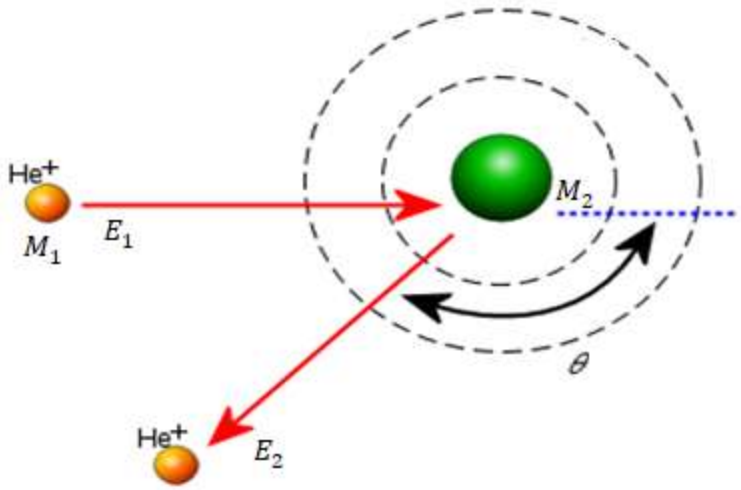

Figure 2. 9: Diagrammatic representation of the RBS principle

The procedure of RBS, involves that ions of detected mass, $M_1$and atomic number, $Z_1$are incident on the target nucleus of mass M_2 and atomic number, Z_2. The backscattered ions are detected. Due to conservation of momentum and energy, the energy E_1 of the scattered ions are determined for a defined scattering angle, θ. The measured energy of back scattered electrons (energy spectrum) describes the elemental composition of target specimen under investigation (Chu.,Mayer and Nicolet, 1978). Considering the kinematics of the collision (the conservation of momentum and kinetic energy), the energy E_1 of the scattered projectile is reduced from the initial energy E_0:

$$E_1 = kE_0 \qquad (2.10)$$

The constant, k is the called the kinematic factor which is a characteristic of the target nucleus.

$$k = \frac{E_1}{E_0} = \left[\frac{\sqrt{M_2^2 - M_1^2 Sin^2\theta} + M_1 COS\,\theta}{M_1 + M_2}\right]^2 \quad (2.11)$$

Particle 1 is the projectile (incident ions), particle 2 is the target nucleus,θ is the scattering angle of the projectile, M_1 is the mass of the projectile, M_2 is the mass of the target nucleus (Chu.,Mayer and Nicolet, 1978). The RBS instrumentation involves three main components:

- An ion source, either alpha particles (He^{2+} ions) or protons
- A linear particle accelerator capable of accelerating incident ions to high energies.
- A detector capable of measuring the energies of ions over some range of angles.

Detectors used to measure backscattered energy are usually silicon surface barrier detectors (Oura; Lifshits; Saranin and Zotov, 2003).

2.6 THE NATIONAL ELECTROSTATIC CORPORATION (NEC) ANALYTICAL ENDSTATION SYSTEM OF THE ACCELERATOR FACILITY AT GAEC.

The NEC analytical endstation is sectioned into four subsystems. These are the vacuum system, detection system, computer system and the manipulator system (www.pelletron.com).

2.6.1 The vacuum system

The vacuum system consists of three gate valves, two rough valves, vent valve, turbo pump, rough pump, turbo pump controller, three thermocouples, ion gauge, convectron

gauge monitor, ion and thermocouple gauge monitor, vacuum interlock controller, and all evacuated space. The vacuum interlock controller directs the position of all valves. On the front panel of the interlock controller there are switches on the front panel of the interlock controller having an auto and closed position for each valve (Pollock, 2015). The controller protects the chamber and pumps by closing valves in during power failure or failure in the vacuum. The controller also prevents the backstreaming of oil from the rough pump into the chamber.

2.6.2 The detection system

The detection system begins with a silicon ion implanted particle detector and other detectors like sodium iodide or HpGe gamma-ray detector, and or Wavelength Dispersive X-Ray detector. Also, high depth resolution magnetic spectrometer detectors have been incorporated with a file extension. The Silicon Surface Barrier (SSB) detector is mounted below the collimator. This gives a scattering angle of 170°. A second SSB detector can be positioned at any angle from outside the vacuum system (Pollock, 2015). Figure 2.10 illustrates the arrangement the various detectors and components in the target chamber.

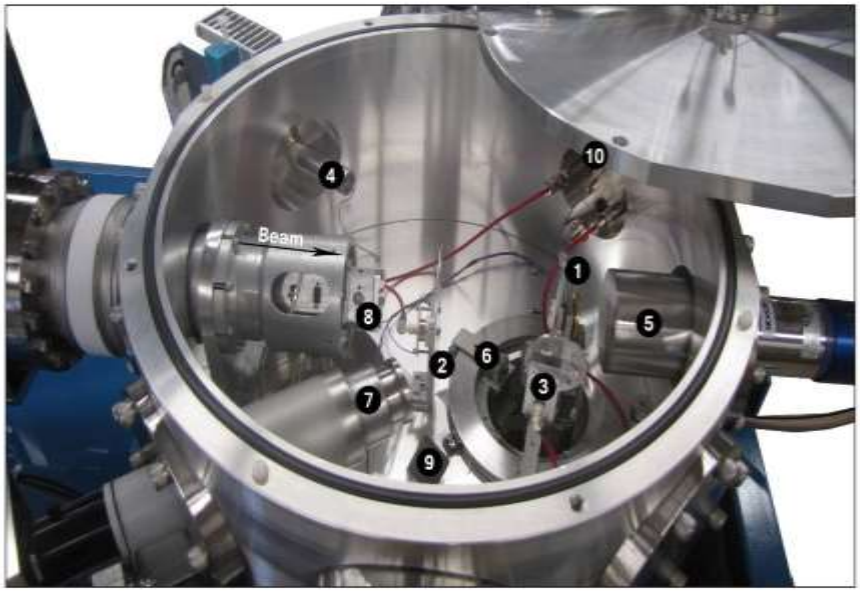

1. Sample
2. Fixed SSB at 170°
3. Moveable SSB and Filters at 180° to 30°
4. X-Ray Detector
5. Gamma Detector at 0°
6. X-Ray Detector Filters
7. Zoom Camera
8. Microprobe Lens
9. Light
10. Chamber Feedthroughs

Figure 2. 10: Representation of the various components in the target chamber (www.pelletron.com)

Each detector has a preamplifier which feeds the signals into a spectroscopy amplifier/digitizer. The signal moves from the preamplifier to the multichannel analyzer/analogue to digital converter. Figure 2.11 represents a schematic arrangement of the detector system.

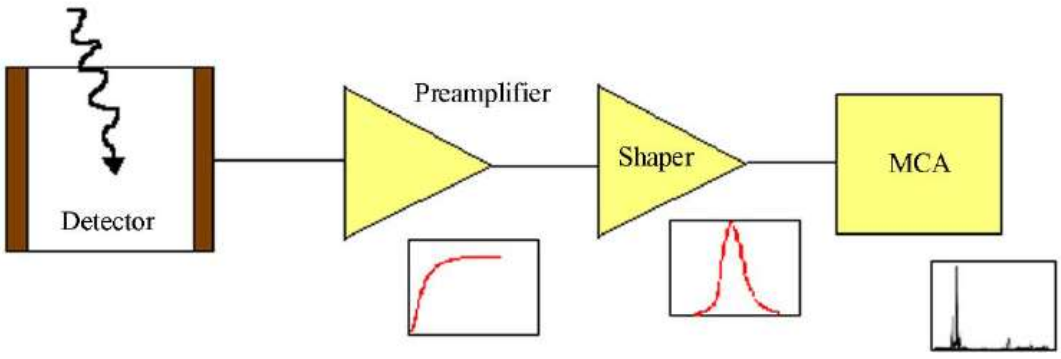

Figure 2. 11: Schematic representation of the detector system

2.6.2.1 The surface barrier detector

As a semiconductor solid-state detector, the surface barrier detector is essentially a p-n junction made out of a silicon (Si) wafer. When an ion travels through the p-n junction, electrons are removed from the Si, and thus slows down. This action continues repeatedly until the charged ion exhausts its kinetic energy and ceases in the Si. The thickness of the Si is required to be enough to stop the ions or particles (Knoll, 2000). The p-n junction is biased such that the produced electrons are collected and subsequently generates a signal indicating the passage of a charged ion.

2.6.3 Manipulator

After all the braces are removed and all electrical motor cables are connected, the limit are switches inspected and adjusted. This is done by moving the motor by hand until it becomes difficult to move. It is moved in the opposite direction about one full turn and the limit switch is adjusted (Pollock, 2015). This is done for all the axes with limit switches.

The RC43.EXE Program is run to set communications between the computer and the controller.

2.6.4 The Computer System

The user can use three software programs to do some of the endstation control, data collection and data analysis of the NEC RC43 analytical system. The three programs have icons displayed on the desktop when the computer is turned on under the Windows OS. These programs are MAESTRO or DppMCA, RC43.EXE and RUMP.EXE or GUPIX.EXE (Pollock, 2015).

2.6.4.1 MAESTRO

This program has the only function of collecting spectra. It has a data collection MCA which gives the user total control of the card's, or digitizer ADC parameters (www.pelletron.com). With this program, growing spectrum is observed. The spectrum is stored to a disk or in different formats and when collection is done.

2.6.4.2 RC43.EXE

This program is a qualitative data collection software used for qualitative analysis and automation of data collection for the RC43 endstation. It does sample manipulation, controls the data collection MCAs, and interfaces with the current integrator, and does qualitative analysis. It also performs automatic data collection for doing channeling, NRA, ERD, PIXE, RBS, and Micro Probe work (Pollock, 2015). This software is also used as an upgrade package for other endstation types. It has several live data displays and writes data to an ASCII file for disk storage.

2.6.4.3 RUMP.EXE

The RUMP.EXE is a data analysis software. There are three subcommand processors in the RUMP program. These are ANNOTE, SIM and PERT. ANNOTE is for labeling plots of spectra. SIM is used to simulate an imaginary sample which is divided into layers. Each layer has a thickness and is composed of at least 1 element. PERT compares a simulated spectrum, made up by the operator, to an actual spectrum collected by the detection system (Pollock, 2015).

2.7 ACCELERATOR ION BEAM ENERGY CALIBRATION

Particle accelerators are often used for both ion implantation and the ion beam analysis, therefore the accurate and precise knowledge of the energies of the accelerated ions is essential. From the analytical point of view, the energy of the accelerated ion needs to be known with a higher precision by calibrating the accelerator (Bachiller-Perea et al., 2013).

There are about three major families of methods used to energy calibrate particle accelerators (Healy, 2006). Some methods are based on accurate detector technologies such as velocity detectors, time-of-flight which requires a complex instrumentation and magnetic analysis (Martin et al, 1985). Another common technique for calibrating the beam energy of particle accelerators are based on reaction thresholds of well characterized gamma resonances or neutron thresholds (Tesmer and Nastasi, 1995).

The non-resonance proton capture technique of particle accelerator beam energy calibration has been reported to directly reveal the beam energy, but this method remains unsuitable for routine use because the cross-sections are so low to give accurate and precise beam energies (Colaux et al, 2015).

An emerging technique utilizes backscattering particles and kinematic scattering factors of different materials (Lane et al, 1993). This method is found to be efficient, simple and cost effective.

Since the inception of particle accelerators, operators of particle accelerators have routinely calibrated their facilities either by one or more of these methods depending on a techniques precision, cost effectiveness and beam time duration. Different facilities employed any of these methods by weighing the advantages and the disadvantages of methods that exist.

Next in this literature are the detail reports on selected techniques of beam energy calibrations of some particle accelerators.

2.7.1 Calibration of ion Beam Energies by Nuclear Resonance and Reaction Thresholds

According to Kureba, nuclear scattering experiments require the energy of the incident beam to be known as accurately as possible and at least to within about 20 keV in order to determine possible resonance energies (Kureba, 2010). The beam energies of most ion accelerators are usually calibrated by using (p,γ) and (α,γ) resonant nuclear reactions.

So many resonant reactions are used during a calibration. These resonant reactions have been tabulated by Marion (Marion, 1966). The region of resonances are found by gradually raising the accelerator voltage and thereby the ion energy (Lane et al, 1993). The observed and true energies of the resonances are then compared to give a calibration curve of ion energy as a function of either the indicated accelerator voltage or the analyzing magnet field (Uhrmacher, Pampus, Bergmeister & Purschke, 1985).

It has also been reported that, the widely established calibration technique remains the use of sharp and well defined nuclear resonances (Brindhaban, Barker, Keeling, & Wood, 1994). Therefore, the most widely used resonant threshold reactions for calibrating the beam energies of particle accelerators are shown in Table 2.2 (Tesmer and Nastasi, 1995).

Table 2. 2: Data on resonant and threshold reactions for accelerator calibration

Incident ion Energy(keV)	Reaction	Key emitted radiation (MeV γ)	Cross section
340.46± 0.04	$^{19}F(p,\alpha\gamma)^{16}O$	6.13	160 mb
872 .1±0.2	$^{19}F(p,\alpha\gamma)^{16}O$	6.13,6.92	540 mb
991.91±0.05	$^{27}Al(p,\gamma)^{28}Si$	1.78	31 ev b
1373.0±1.0	$^{19}F(p,\alpha\gamma)^{16}O$	6.13	300 mb
1747.6± 0.9	$^{13}C(P,\gamma)^{14}N$	9.17	340 mb
2437.4±1.0	$^{24}Mg(\alpha,\gamma)^{28}Si$	12.07	Unknown
2868±2.0	$^{24}Mg(\alpha,\gamma)^{28}Si$	12.44	Unknown

It has also been reported in a related work that, narrow resonant widths only afford accurate calibration provided the beam energy is stable and the sample surface is not contaminated (Healy, 2006). Most research works aimed in calibrating particle accelerator systems used the shapes of proton backscattering spectra from silicon, which are characteristic of the beam energy, as a key for calibrating those accelerator systems (Gurbich 1998).

The γ-ray decay from the Ep = 992 keV resonance in the $^{27}Al\ (p,\gamma)\ ^{28}Si$ reaction has been studied in the past by numerous groups. The intensity and energies of γ-rays produced via the Ep=992 keV proton capture resonance in the $^{27}Al\ (p,\gamma)\ ^{28}Si$ resonance were found to be useful for calibration of small ion accelerators. For, (p,γ) reaction studies one often obtains gamma rays in the energy region 0.5-10.0 MeV, due to the high Q-value for these reactions (Scott & Lusby,1975).

Kelly reported that, the best method to get an accurate calibration of accelerator beam energies in the MeV-range is to employ the beam to produce nuclear reactions that occur at known and accurate measured energies. The appropriate resonance reaction as reported

is the $^{27}Al + p \rightarrow {}^{28}Si^*$, where the ^{28}Si nucleus is excited by the incident energetic protons to emit gamma radiation. The defined resonance occurs at an incident proton energy of 991.88 keV. (Kelly, 2000).

Also, the Surrey Ion Beam Centre has recently made routine use of this elastic $^{16}O(\alpha,\alpha)^{16}O$ reaction resonance at 3038 keV to calibrate their beam energy and chain of detection. It was experimentally demonstrated that, the beam energy can be determined at remarkably good precision with this method. The accuracy of this method was mainly limited by the accuracy at which the energy of the resonance was known. It was determined from the beam energy calibration that, the energy of this resonance was 3038.2 ± 3.1 (Colaux et al., 2015).

2.7.2 Ion Beam Energy Calibration of Particle Accelerators by Magnetic Analysis

The magnetic method of ion beam energy calibration implies noting the analyzing magnet field strengths needed to transmit a number of beams of different isotopes simultaneously produced within the accelerator. A constant of proportionality between the analyzing magnet field and the square root of the ion energy is then calculated. Calibration by this technique can be achieved within 24 hours beam time, although the resulting calibration constant can be nonlinear on some accelerator systems if a wide energy range is examined (Shamu, Bernstein & Parrot, 1973).

It is worth noting that, few accelerators are equipped with absolute systems for measuring the beam energy. Therefore, nuclear reaction experiments are performed with energy analyzers that require calibration. A calibrated momentum-analyzing magnet system determines the absolute energy of an ion beam from an accelerator. Detailed field or beam

measurements must be carried out in order to achieve the needed magnet calibration. (Olsen et al., 1987).

A common procedure for calibrating the analyzing magnet of a tandem Van de Graaff accelerator requires that measurement of neutron threshold energies is done. Threshold energies have been determined from absolute measurements of the incident particle energy for a number of reactions and have been tabulated for calibration purposes (Marion, 1966). It is noted that, a more convenient way for measuring neutron threshold energies is to observe the emitted neutrons at 0 ° using a simple neutron detector such as a long counter. This procedure can be done with (p,n) reactions, for example, up to 6 MeV.

Another basic way for determining beam energies at many accelerator facilities is to measure the magnetic field required to bend the beam through a magnetic analysis system. Calibration of such a system has always been completed by performing detailed magnetic field measurements using a Hall probe, a flip coil or a nuclear magnetic resonance (NMR) probe. These measurements then allow the calculation of particle trajectories through the system. The floating wire technique has allowed simulation of particle trajectories directly and has been developed to accuracies comparable to that attainable by magnetic field mapping (Bischscl, 1965). By this procedure, measurements are made over the full range of magnet excitation because of possible saturation effects (Gross, 1976).

The FN-tandem accelerator in Bucharest was commissioned in March 1973 but its operation was stopped for long time period, due to the strong earthquakes in Romania in 1977 and 1986. In 2006 a program of modernization and development of the accelerator was started. Because of this, it became necessary that, an NMR fluxmeter for measuring the magnetic field in the analyzing magnet gap was installed. In the light of this

development, calibration of the energy analyzing system (analyzing magnet) of the Bucharest tandem accelerator was needed. Subsequently, an energy calibration of the analyzing magnet of the Bucharest tandem was completed by comparing the energies of alpha particles from a ^{241}Am source with the energies of ^{4}He projectiles back-scattered by thin carbon and gold layers. This result was found to be in agreement with the results of previous calibrations done on this facility. The measurements were performed with a standard backscattering, using $^{4}H^{++}$ ion beams from the 9 MV tandem Van de Graaff accelerator (Roxana et al., 2012).

2.7.3 Emerging Techniques for Calibrating the Beam Energies of Particle Accelerators

There have been a lot of emerging methods used to calibrate energies of beams produced by particle accelerators. Emerging techniques, mostly based on the principles of RBS are convenient, efficient, and are very fast.

A technique based on the measurement of elastic and inelastic proton scattering (Scott & Paine, 1983); obtaining the calibration constant with a moderate accuracy has been produced. This was achieved by bombarding a thin target of ^{11}B with protons at two different accelerator energies. The result contained in the elastic and inelastic measured spectra proved enough to determining the spectrometer channel width and energy calibration constant as well as the beam energy (Bachiller-Perea et al., 2013).

Another alternative but simple method of calibrating the beam energies of an accelerator has been established. Accelerated ions from a 2.5 MV Van de Graaff generator were elastically scattered (by the principles of RBS) from a number of known targets, and their

measured energies were compared to that for the known energy of α particles from a thin layer ^{241}Am source.

This calibration procedure provided an accurate calibration for the generating voltmeter of the accelerator. Finally, the true energy E, in electron volts, of an accelerated beam of this accelerator system was achieved and as represented by the model equation:

$$E = -0.013n + 1.014nV_m \text{ (MeV)} \quad (2.12)$$

V_m = the accelerator voltage as measured by the generating voltmeter.

The calibration procedure has been tested against and found to be in good agreement with published $^{19}F(p,\alpha\gamma)^{16}0$ nuclear reaction resonance data. (Lane et al, 1993).

CHAPTER 3

MATERIALS AND METHODOLOGY

3.1 MATERIALS

Figure 3.1 shows the 1.7 MV NEC 5SHD-2 model Pelletron Accelerator facility at GAEC.

Figure 3. 1: Setup of the 1.7 MV Pelletron accelerator at the Ghana Atomic Energy Commission

In order to successfully perform the ion beam energy calibration for the 1.7 MV tandem accelerator, the following materials were used:

i. Thin target standard reference materials with thickness of about 10 $\mu g/cm^2$ of copper, gold, silicon and Aluminum as shown in figure 3.2. The gold target is mounted on glass substrate.

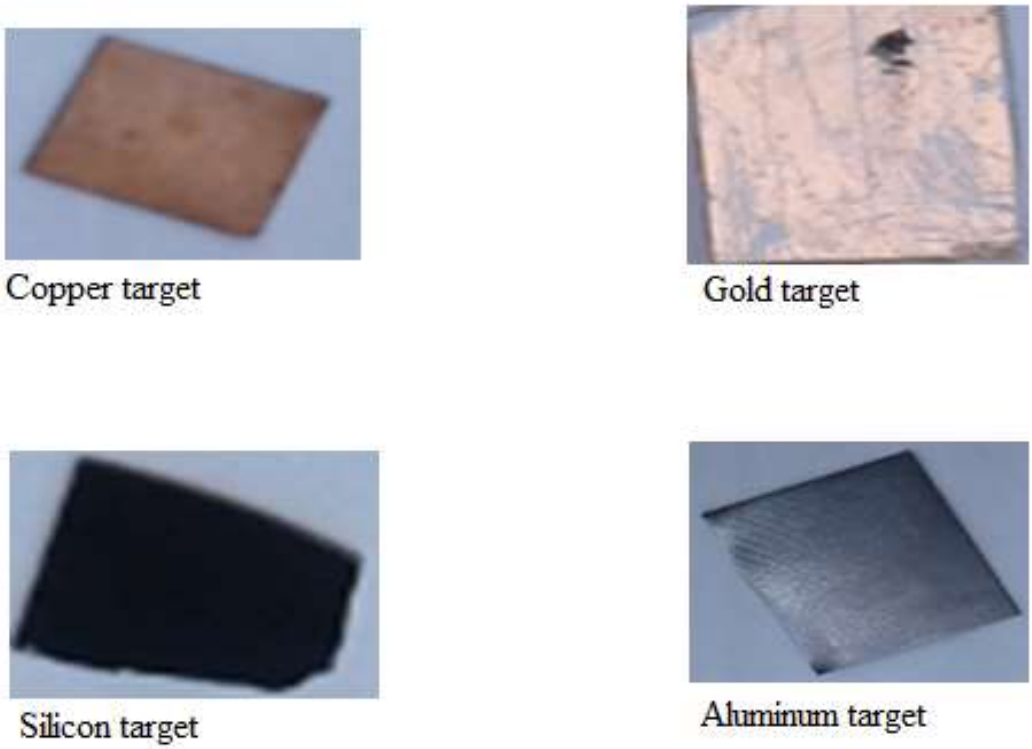

Figure 3. 2: Standard reference target materials of Copper, Gold, Silicon and Aluminum

ii. ^{241}Am 5.486 MeV Alpha (α)-radiation source of 666 Bq as activity at the time of counting as shown in figure 3.3.

Figure 3. 3: 241_{Am} 5.486 MeV Alpha α radiation source

3.2 IRRADIATION AND SPECTRUM COLLECTION OF SAMPLES

Irradiation of all target materials used in this study was done using the accelerator facility at the ARC center.

Spectra were acquired from the irradiated samples using the RC43 Analytical Data collection software.

3.3 THEORY OF METHODOLOGY

This is a simple method of calibrating the Helium beam energy of this pelletron/ tandem accelerator system. The theory has to do with initial calibrations of the detector and the accelerator; making up the accelerator system calibration.

This means of calibration is achieved by complying with the theories below. The actual energy E (eV), of an accelerated ion is given as:

$$E = nV_O + n\alpha V_m \qquad (3.1)$$

Where $\boldsymbol{V}_o$= systematic offset that might be in voltage scale, n= the charge ion state of the particle, $\boldsymbol{\alpha}$=constant of the voltmeter and $\boldsymbol{V_m}$= accelerator voltage measured by the generating voltmeter. $\boldsymbol{V}_o$ and $\boldsymbol{\alpha}$ are the calibration constants to be determined.

The detection system calibration is done in relation to the Multi-Channel Analyzer (MCA) channel number C. By this way, ions of particular energy E are detected after they have been scattered from the surface of a material target. This procedure is characterized by a Rutherford backscattering kinematic factor, k. Therefore, C is given as:

$$C = C_O + \beta kE \qquad (3.2)$$

Where, $\boldsymbol{C_o}$ =any possible systematic offset that might be in the MCA, k = Rutherford backscattering kinematic factor, E in equation 2.13 is the energy of the detected ions, $\boldsymbol{\beta}$ = constant of the detection system which is mostly an inherent property of the detector system and kE = the actual energy of the scattered ions.

Adding eqn. (3.1) and eqn. (3.2),

$$C = C_O + nk\beta(V_O + \alpha V_m) \quad (3.3)$$

The total energy calibration of the accelerator is done by employing equation (3.1). However, the detection of a particle of known energy completes the energy calibration procedure. A typical example is the use of alpha particles from ^{241}Am of energy E_{Am}. In this case, eqn. (3.2) is transformed to offer the channel for detection as $C_{Am.}$

$$C_{Am} = C_o + \beta E_{Am} \quad (3.4)$$

3.4 THE CALIBRATION PROCEDURE

Helium beam of charge state, n = 2 is used for this calibration. The Amptek silicon surface barrier detector is placed at a scattering angle of 165^o to help detect the ions that are backscattered from the interaction with the target materials (samples).

Calibration of both the ion acceleration and target detector-systems were carried out separately and later combined to achieve the overall ion beam energy calibration.

Figure 3.4 is the flow chart of the energy calibration methodology utilized for this work (Lane et al, 1993).

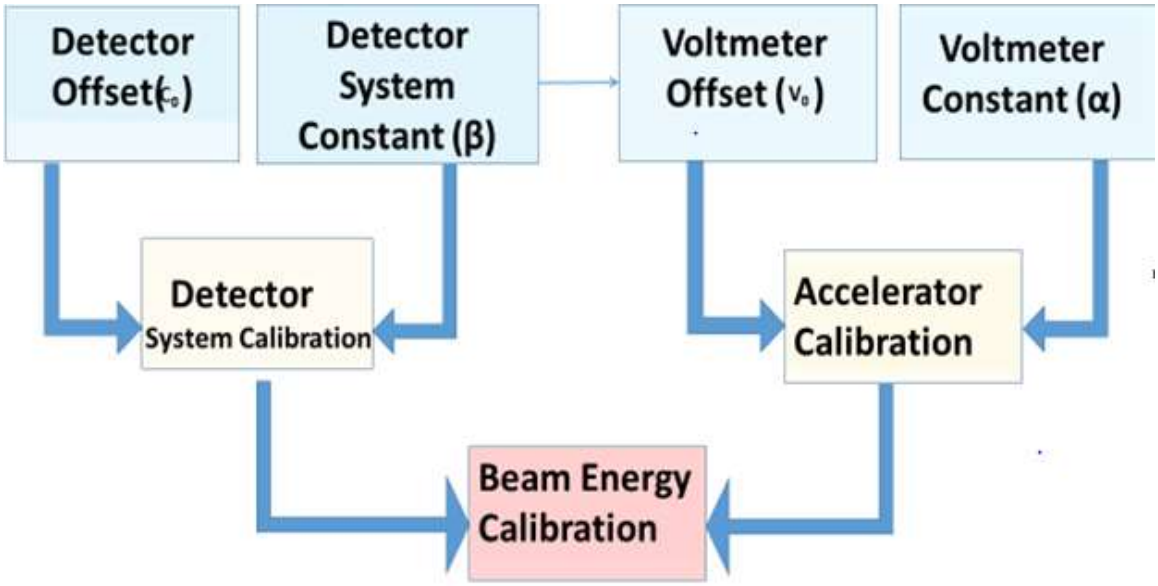

Figure 3. 4: Flow chart of the methodology

3.4.1 Calibration of the detector system

The calibration of the detector was accomplished by experimentally determining the detector offset (C_o) and the detection system constant (β).

3.4.1.1 Detector Offset (C_o) determination

The four targets materials, aluminum, copper, gold and silicon were irradiated with helium beam under constant accelerating voltage of 0.6688 MV. An RBS spectrum was collected for each of the targets at a collection charge of 20 µC. These spectra were fitted with the Simulation of Non-Rutherford Backscattering Nuclear Reaction Analysis (SIMNRA) quantitative software and the kinematic factor for each target reaction determined. During the fitting process, each target element is energy calibrated to place the channel of detection of each target element to its corresponding energy. This is done by gradually adjusting the

energy per channel and particles solid angle parameters in the SIMNRA software. The channel of detection, C for backscattered α particles for each target element were recorded. The kinematic factor of each of the target material was determined by using the relation:

$$k = \frac{E_1}{E_0} \qquad (3.1)$$

Where E_0 = initial or incident energy of the α particles and E_1= backscattered energy of the scattered α particles. A graph of channel of detection (C) of the individual target elements is plotted against their respective kinematic, k, factors. A straight line is fitted and the intercept, C_o which reveals the systematic offset in the detector.

3.4.1.2 Detector system constant (β) determination

The detector system calibration is completed by observing the channel for detecting alpha particle from the ^{241}Am radioactive source.

The ^{241}Am (5.486 MeV α source) is placed 1cm close to the detector in the vacuum chamber so as to cause an interaction between the detector and the americium source. RBS spectrum for the alpha source is acquired by importing the ASCII saved files of the interaction into the SIMNRA software. The channel number, C_{Am} for detecting the 5.486 MeV α source is read and recorded.

Since all parameters are known, the constant of the detection medium, β is determined to as:

$$\beta = \frac{C_{Am} - C_0}{E_{Am}} \qquad (3.2)$$

At this stage, the detector system calibration is achieved

3.4.2 ACCELERATOR CALIBRATION

It was ensured that the accelerator and voltmeter have stabilized before the calibration process was initiated. The silicon surface barrier detector was placed at an angle of 165° to detect the alpha particles that are backscattered.

At this stage of the calibration, gold target is used as the only target material and backscattering spectra were collected at five measured accelerator voltages, V_m = 0.4 MV, 0.7 MV, 0.9 MV, 1.096 MV and 1.198 MV.

The gold target is irradiated with helium beam of accelerating voltage, 0.4 MV. The backscattered α particles are detected with the surface barrier detector. An RBS spectrum was collected for the gold target at a collection charge of 20 μC. This spectrum was fitted with the SIMNRA quantitative software. During the fitting process, the gold element is energy calibrated to place its channel of detection to the corresponding energy. This is done by gradually adjusting the energy per channel and particles solid angle parameters in the SIMNRA software. The channel of detection, C was read and recorded for backscattered α-particles for the gold target at this accelerating voltage.

Maintaining the gold target, the alpha particle accelerating voltage is varied at voltmeter readings (V_m) of 0.7 MV, 0.9 MV, 1.096 MV and 1.198 MV. At each accelerating voltage, an RBS spectrum was collected for the gold target at a collection charge of 20 μC. Each spectrum was fitted using the SIMNRA quantitative software. During the fitting process for the four different spectra, the gold element is energy calibrated to place the channels of detection to their corresponding energies. This is done by gradually adjusting the energy per channel and particles solid angle parameters in the SIMNRA software. The channels

of detection, C were separately read and recorded for backscattered α particles for the gold target at the four different accelerating voltages.

From the resulting data, a graph of C is plotted against V_m as shown in equation 3.3.

$$C = (C_O + nk\beta V_O) + nk\alpha\beta V_m \tag{3.3}$$

Using the earlier known and computed values of β and C_O, the k value of Au and n=2, the calibration constants, V_o and α are determined from the graph:

$$V_o = \frac{Intercept - C_O}{k\beta} \tag{3.4}$$

$$\alpha = \frac{Slope}{k\beta} \tag{3.5}$$

After all these constants are determined, the calibration is completed.

CHAPTER 4

RESULTS AND DISCUSSIONS

4.1 OVERVIEW

This chapter presents the results and discussions on the various procedures followed to achieve the ion beam energy calibration of this accelerator facility.

4.2 DETECTOR SYSTEM CALIBRATION

The first stage of the calibration was achieved by determining the detector offset (C_o) and the detection system constant (β). Therefore, the results of the detector offset (C_o) and the detection system constant (β) are presented. The raw spectrum is represented by the red curve whereas the fitted spectrum is represented by the blue spectrum.

4.2.1 Detector Offset (C_o) determination

Figure 4.1 represents the raw (undeconvoluted) spectrum generated after the recorded ASCII data of gold target irradiated at the accelerator terminal voltage of 0.6688 MV was imported into SIMNRA software.

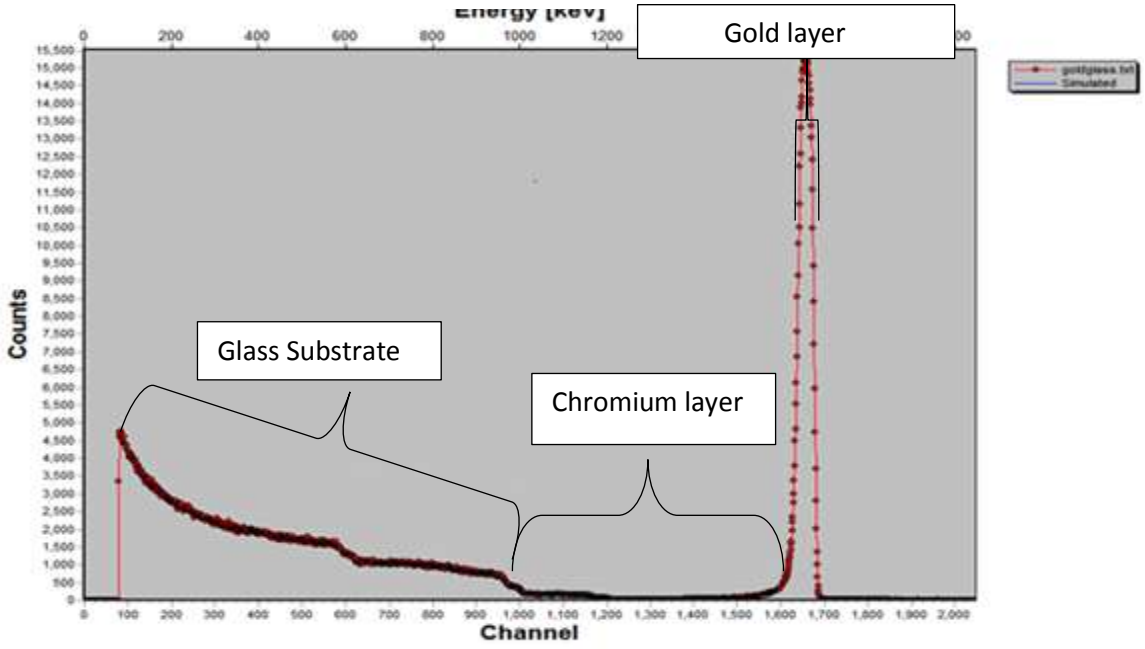

Figure 4. 1: Raw (undeconvoluted) SIMNRA spectrum for gold target at accelerator terminal voltage of 0.6688 MV

In figure 4.1, the gold peak is observed to be thin as compared to the glass substrate. This is because the scattered energy during the particle interaction with the gold sample is less. The gold peak showed a higher peak count of 1500 because a lot of interactions occurred between the helium beam and the gold sample. Also, the broad curve indicates the glass substrate of gold. This broad curve was observed because the difference in the scattered peak was higher. Also, interactions that occurred within the glass sample was very less resulting a lesser peak count of 4500. The plateau formed indicates a separation between the two overlapping peaks of gold and glass; revealing the chromium thin layer sandwiched between the glass substrate and the gold target. Therefore, the plateau or the observed drastic fall in counts indicates a very less interaction between the helium beam and the thin chromium layer.

Figure 4.1 was calibrated so that the channels matched their true energies. In so doing, the following adjustments were carried out: the energy to channel ratio was set to 1.12 keV/ch and the solid angle set at 3.7×10^{11} particles sr. Parameters such as energy spread, calibration offset, and detector resolution were not altered. The spectrum fitting parameters for the gold target at this accelerator terminal voltage of 0.6688 MV is shown in figure 4.2

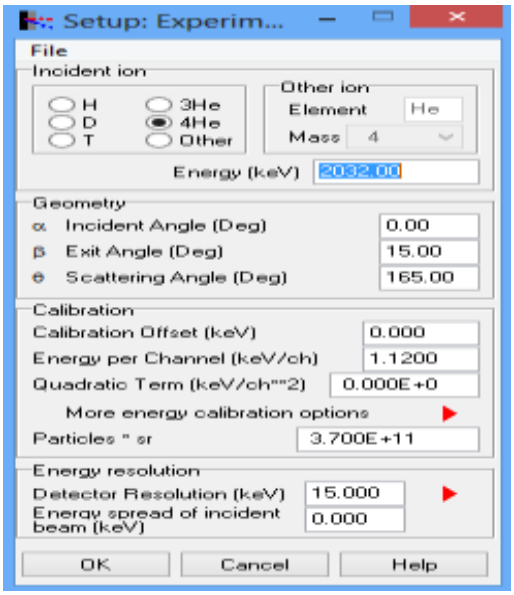

Figure 4. 2: Calibration parameters for Gold at accelerator terminal voltage of 0.6688 MV

After the necessary adjustments, the gold spectrum was fitted with a simulated spectrum that closely matched the raw spectrum. As observed in figure 4.3, channels of detection are matched to their true energies.

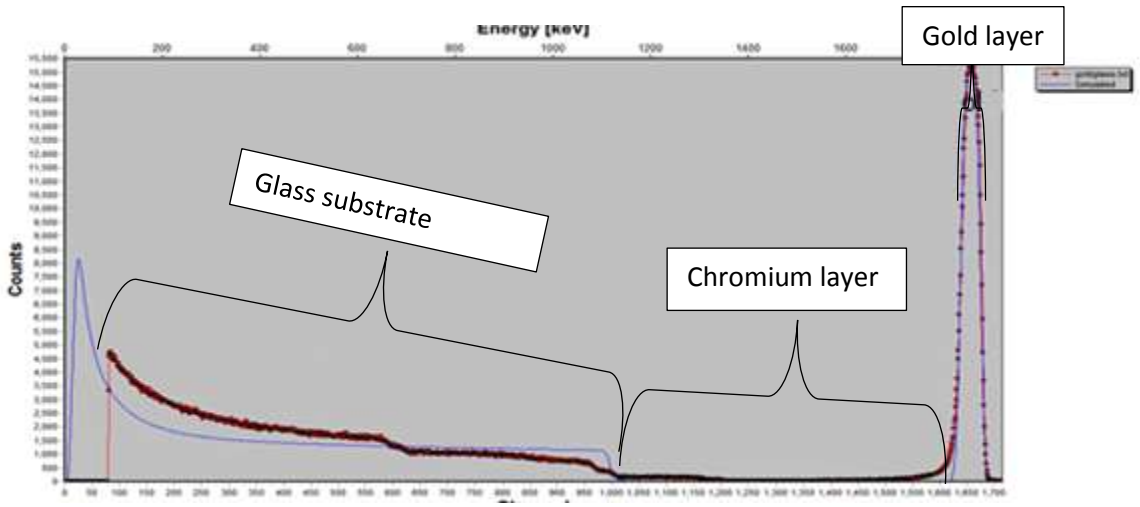

Figure 4. 3: The Calibrated SIMNRA spectrum for gold target at accelerator terminal voltage of 0.6688 MV

After the spectrum fitting process, the channel for detecting the gold sample was found to be at channel 1658.

In figure 4.3, the red curve indicates the raw or the experimentally generated spectrum of gold target and the blue curve indicates the calibrated or the simulated spectrum of the gold target. The experimental and the calibrated gold (Au) peaks matched perfectly due to purity of the gold sample. The glass substrate end of the raw spectrum was not fitted as this was not part of the region of interest (ROI); hence the difference observed in the curves at the region.

Figure 4.4 shows the raw (undeconvoluted) spectrum of aluminum generated after the ASCII data of aluminum target at accelerator terminal voltage of 0.6688 MV was imported into SIMNRA software.

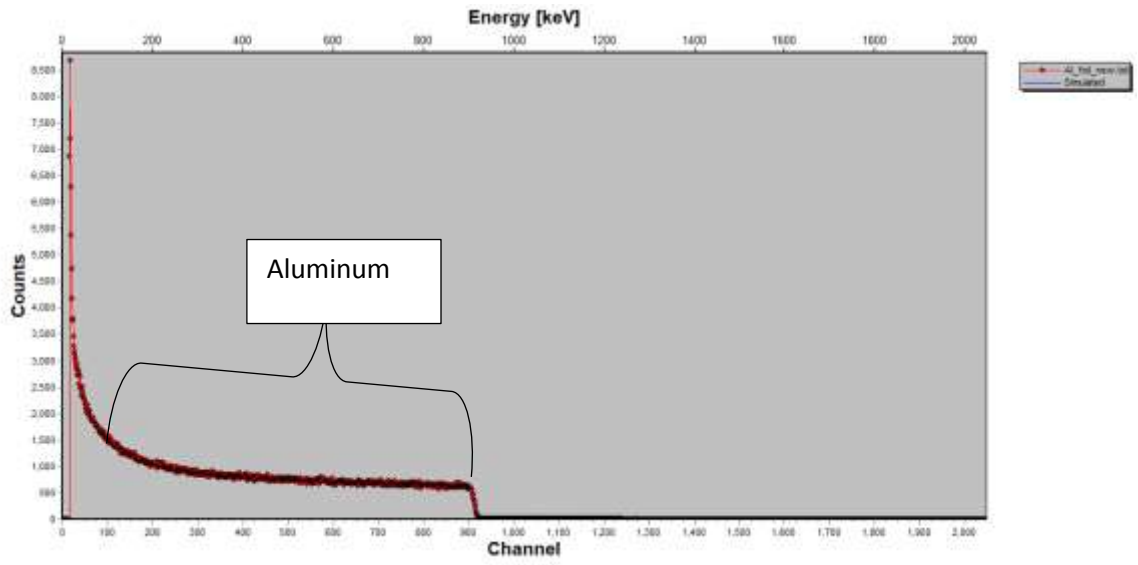

Figure 4. 4: Raw (undeconvoluted) SIMNRA spectrum for aluminum at 0.6688 MV

As the helium beam interacted with the aluminum target, the energy of the helium beams continuously reduced between the counts of 8500 to 1000. This accounted for the scattered points in the aluminum target.

The difference in scattered energy is very high in the aluminum target. This indicates that a lot of the aluminum atoms are concentrated at the latter end of the target and hence less interactions are observed in this sample.

The aluminum spectrum in figure 4.4 was fitted so that the channels matched their true energies. In fitting the aluminum spectrum, all other parameters remained unchanged but the particles solid angle was adjusted to 2.0 $x10^{11}$ particles and the energy per channel ratio set at 1.218 KeV/Ch. This is as shown in figure 4.5

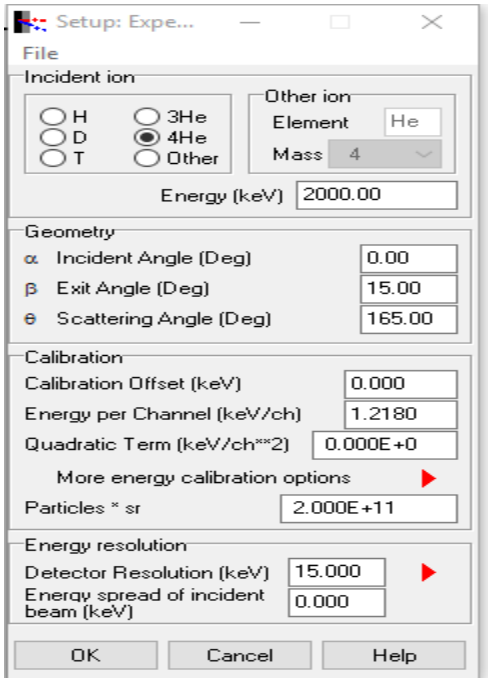

Figure 4. 5: Calibration parameters for aluminum at accelerator terminal voltage of 0.6688 MV

It is observed in figure 4.6 that, after the spectrum fitting process, the corresponding energies of the aluminum target were matched to their true channels of detection.

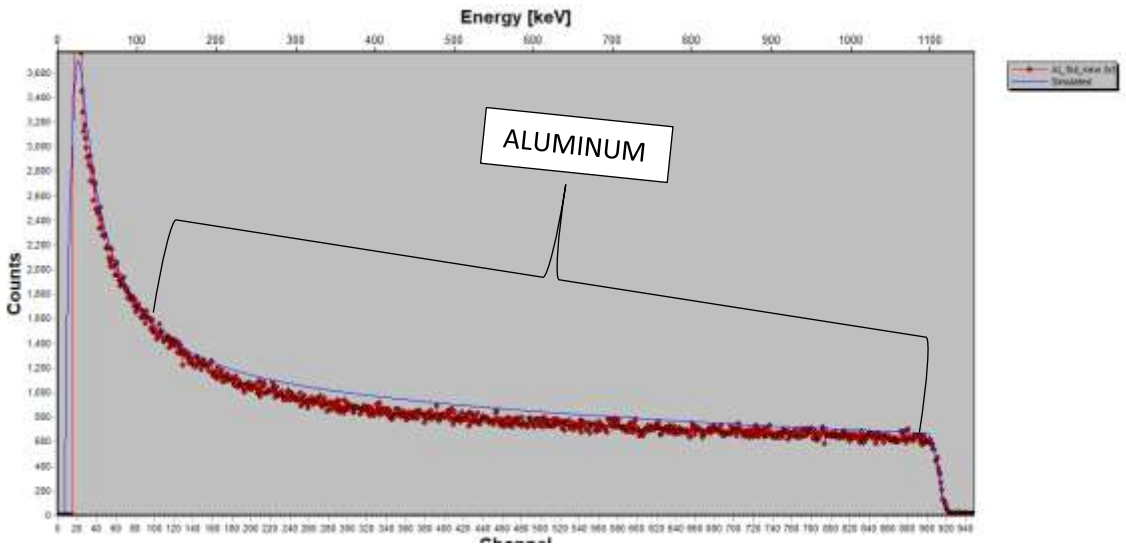

Figure 4. 6: Calibrated SIMNRA spectrum for aluminum at accelerator terminal voltage of 0.6688 MV

The red curve represents the experimental or the uncalibrated spectrum of the aluminum target whereas the blue curve represents the calibrated or simulated spectrum of the aluminum target.

The number of counts obtained from the simulated spectrum was 3700 and that of the experimental spectrum was a little above 3700. There is no noticeable deviation between the simulated and the experimental counts. This confirms that the target material is a pure aluminum target. Also, more of the aluminum atoms are located deep within the aluminum other than its surface.

After the spectrum fitting process, the channel for detecting the aluminum sample was found to be at channel 992.

Figure 4.7 shows the raw (undeconvoluted) copper spectrum after the ASCII data for copper at accelerator terminal voltage of 0.6688 MV was imported into SIMNRA software.

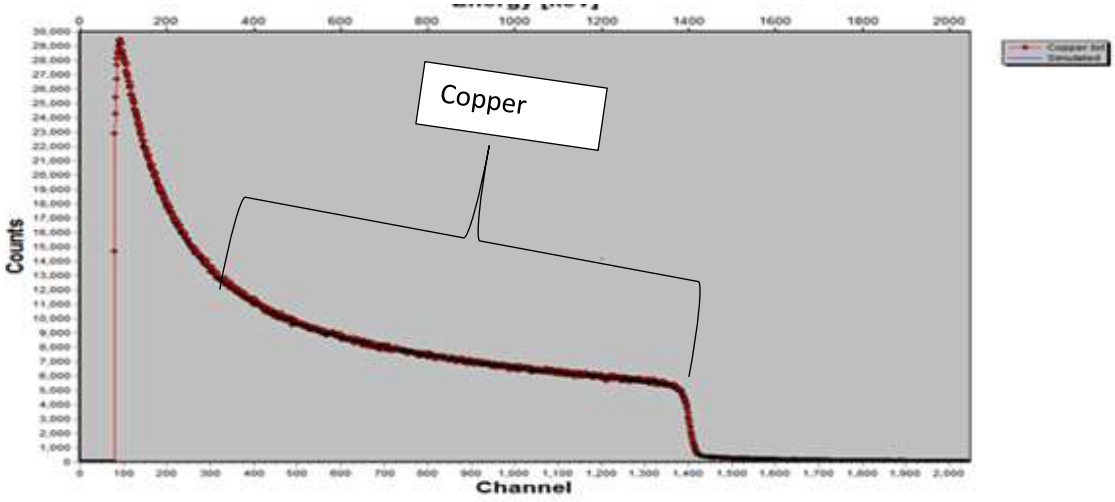

Figure 4. 7: Raw (undeconvoluted) SIMNRA spectrum for copper at accelerator terminal voltage at 0.6688 MV

More of the copper atoms or particles are concentrated at the base of the target and hence less interactions are observed in this sample. This resulted in little or no observed scattered points in the copper target.

The copper spectrum was fitted by adjusting the energy to channel ratio to 1.13 keV/ch and the solid angle set at 5.5×10^{11} particles sr. Parameters such as energy spread, calibration offset, and detector resolution were not altered. The calibration parameters for the copper target at this voltage of 0.6688 MV is shown in figure 4.8

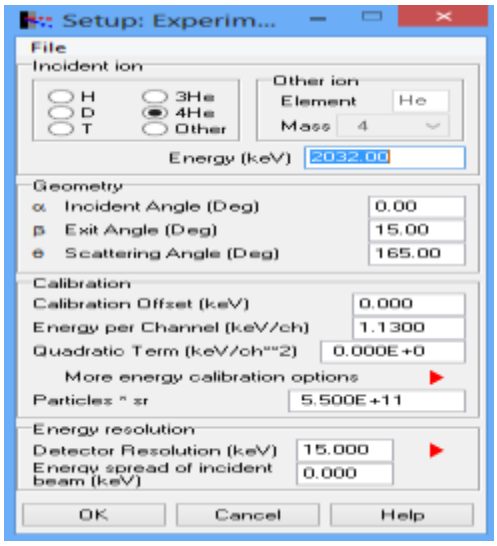

Figure 4. 8: Calibration parameters for copper at accelerator terminal voltage of 0.6688 MV

After the calibration parameters were adjusted, the copper spectrum was calibrated. Figure 4.9 shows the fitted spectrum of copper.

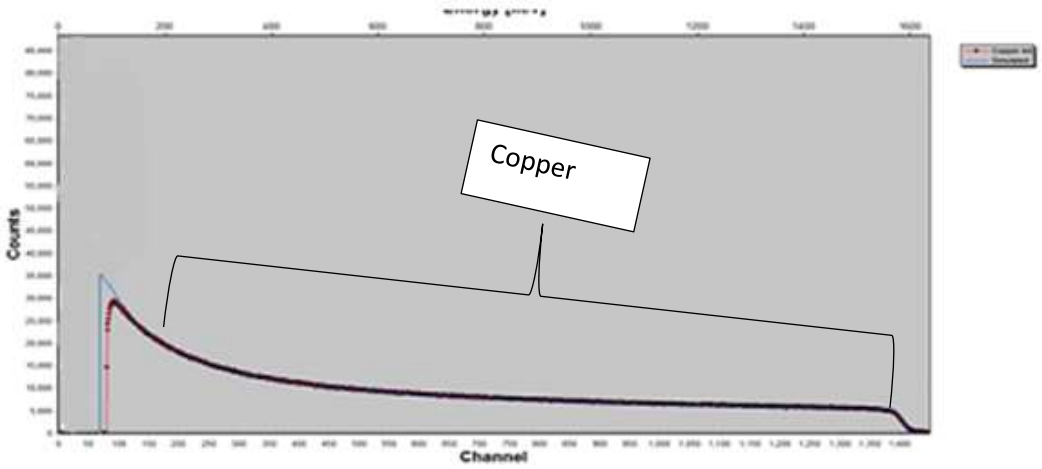

Figure 4. 9: Calibrated SIMNRA spectrum for copper at accelerator terminal voltage of 0.6688 MV

The count of the theoretical simulation (the blue curve) was 40000 and that of the experimental simulation (red curve) was 30000. The deviation in count is negligible, indicating that the target is a pure copper target.

After the spectrum fitting process, the channel for detecting the copper sample was found to be at channel 1414.

Figure 4.10 shows the raw (undeconvoluted) silicon spectrum generated after the ASCII data of silicon at 0.6688 MV was imported into SIMNRA software.

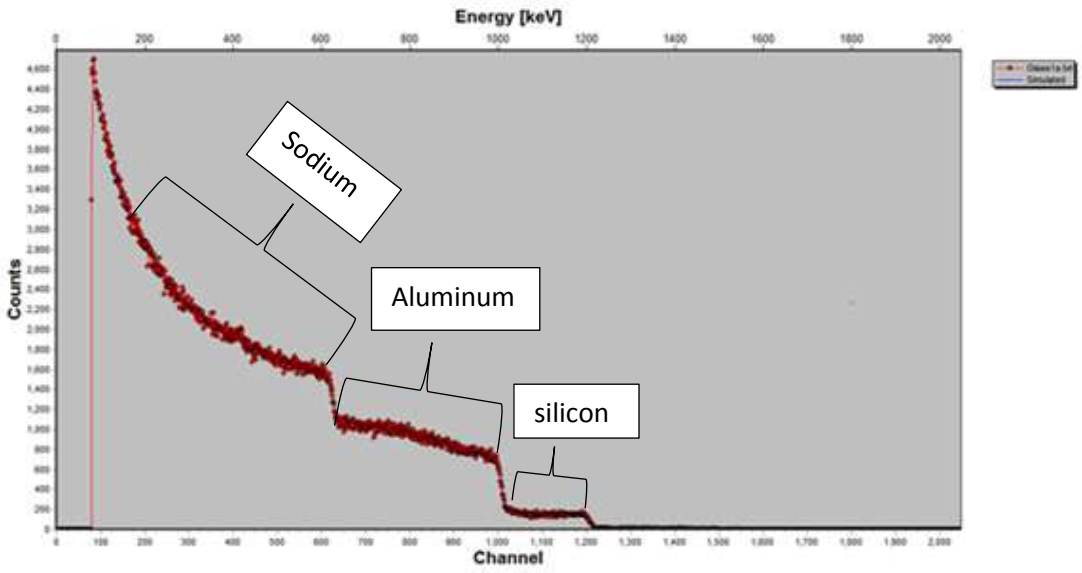

Figure 4. 10: Raw (undeconvoluted) SIMNRA spectrum for silicon target at accelerator terminal voltage of 0.6688 MV

More atoms of glass are concentrated at the base of the target and hence less interactions are observed in this sample. This resulted in an observed peak count of about 4000.

The steps in the curve indicates that the silicon target is not homogenous; owing to the fact that other trace elements may be present in silicon material.

The spectrum in figure 4.10 is fitted by adjusting the energy to channel ratio to 1.15 keV/ch and the solid angle set at 5.5×10^{11} particles sr. The energy spread, calibration offset, detector resolution parameters were not altered. The fitting parameters for the silicon target at this voltage of 0.6688 MV is shown in figure 4.11.

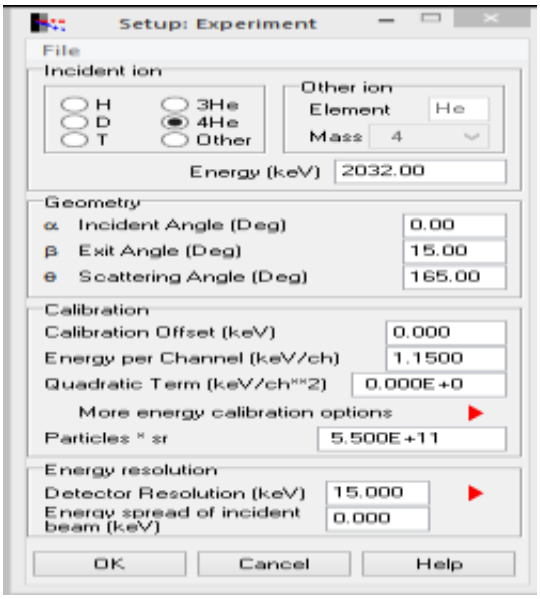

Figure 4. 11: Calibration parameters for silicon target at accelerator terminal voltage of 0.6688 MV

After the adjustments, the channels are matched to their respective energies. As observed in figure 4.12, the count of the theoretical simulation (the blue curve) was 95000 and that of the experimental simulation (the red curve) was 4500.

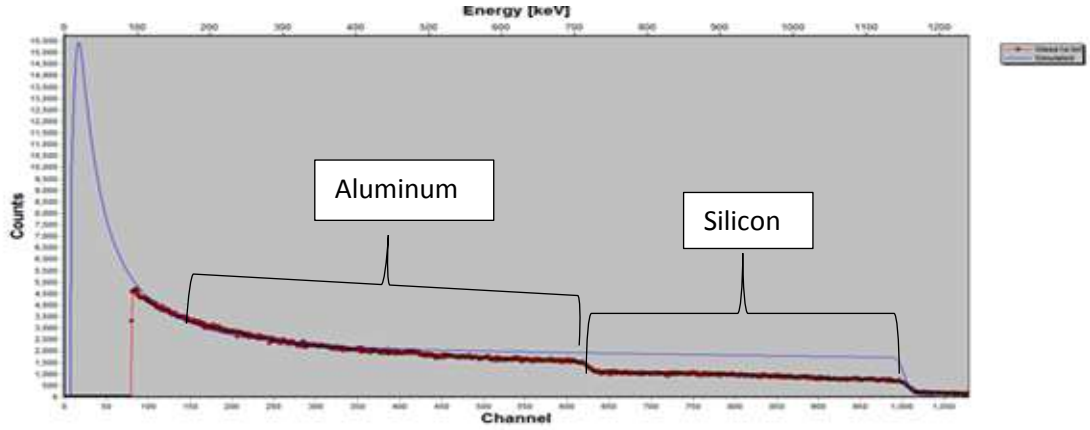

Figure 4. 12: Calibrated SIMNRA spectrum for silicon at accelerator terminal voltage of 0.6688 MV

The deviations in the counts is as a result of the inhomogeneity of the silicon sample. The suspected trace elements (aluminum and sodium) that are in the silicon sample caused scattering and energy loss as the helium beam interacted with the silicon target at a terminal voltage of 0.6688 MV.

After the fitting process, the channel for detecting the silicon sample was found to be at channel 1012.

The channels for detecting each of target elements; gold, aluminum, copper, and silicon after the calibrations are recorded in table 4.1. It is observed that he channels of detection increased as the accelerator voltage increased. Also, the scattered energy of each target element is also recorded in table 4.1.

The RBS kinematic factor for each target material was calculated using the relation,

$$k = \frac{E_1}{E_0} \qquad (4.1)$$

Where E_0 = initial energy of the α particles (E_0= 2032.00keV) and E_1= backscattered energy of the scattered α particles. Also, the calculated values of the kinematic factors of the Gold, Aluminum, Copper, Glass and silicon targets are recorded in table 4.1.

Table 4. 1: Experimental data for scattered energies of α particles, channel numbers and kinematic factors of the different target materials

Element	E_1(keV)	Energy/Channel offset (KeV/Ch)	Channel number, C	Kinematic factor, K
Aluminum	1141.38	1.22	992	0.5617
Silicon	1141.38	1.12	1012	0.573
Copper	1164.38	1.15	1414	0.7866
Gold	1857.52	1.15	1658	0.9141

The result of a linear plot of channel number against kinematic factor is shown in figure 4.13. From this plot, the kinematic factors and the channels of observing a target element are directly proportional. Also, the intercept reveals the detector offset (C_0) as -70.24.

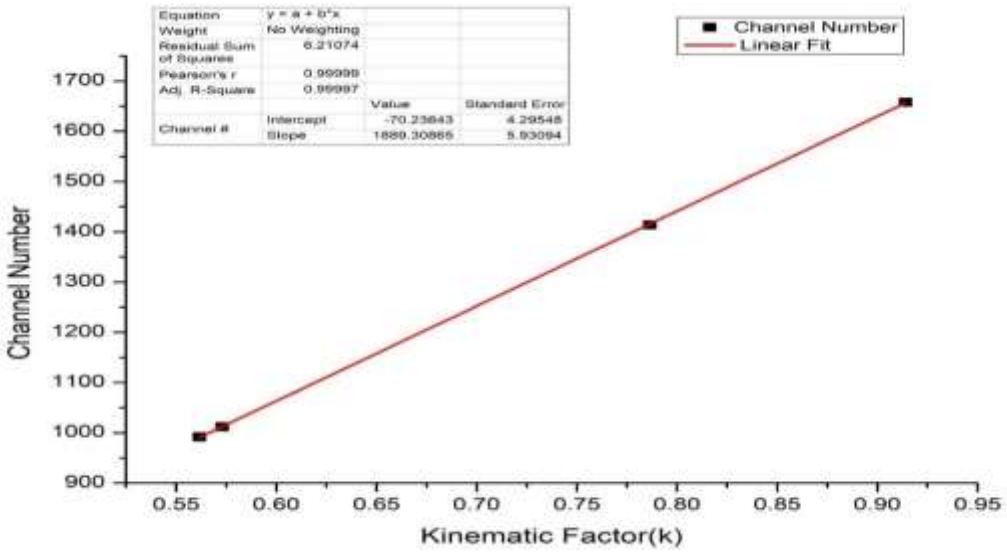

Figure 4. 13: Calibration graph of channel numbers (C) plotted against kinematic factors (k)

4.2.2. Determination of the detection system constant (β).

Figure 4.14 shows the experimental spectrum of the americium source.

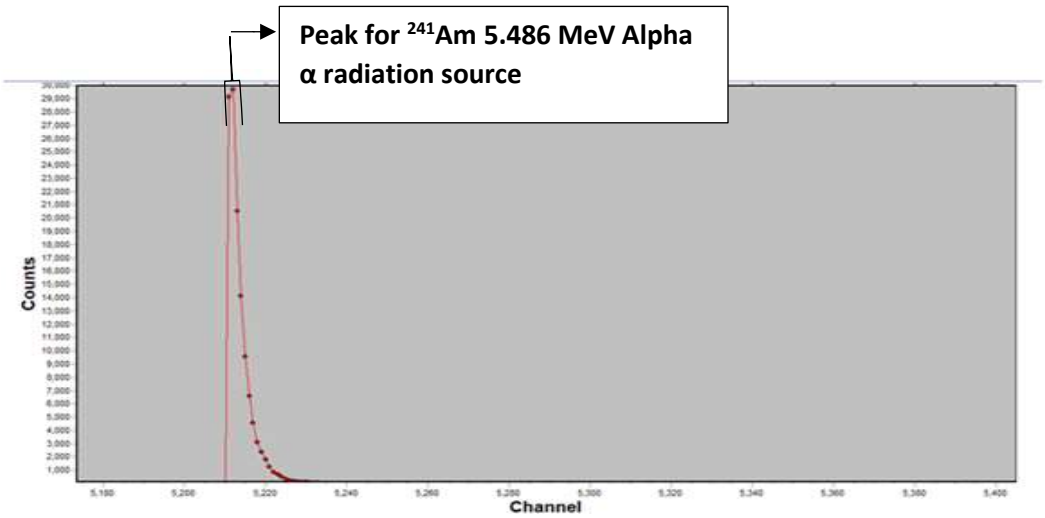

Figure 4. 14: Spectrum for the ^{241}Am 5.486 MeV Alpha α radiation source

At a count of about 30000, the channel C_{Am} for observing the 5.486 MeV alpha radiation has been found to be 5212.

The energy, E_{Am} of the americium alpha source is 5.486 MeV. Also, with C_{Am} and C_o known, the detection system constant, β is determined as;

$$\beta = \frac{C_{Am} - C_0}{E_{Am}} = \frac{5212 - (-70.24)}{5.486} = 962.8 \text{ channels/MeV} \qquad (4.2)$$

This completes the detection system calibration.

4.3: ACCELERATOR SYSTEM CALIBRATION

The results and discussions of the generated spectra when helium beam accelerated at five different accelerating voltages; 0.4 MV,0.7 MV,0.9 MV,1.096 MV and 1.198 MV interacted with the gold target are presented in this section.

Figure 4.15 represents the raw (undeconvoluted) spectrum generated when helium beam accelerated at 0.4 MV interacted with the gold target.

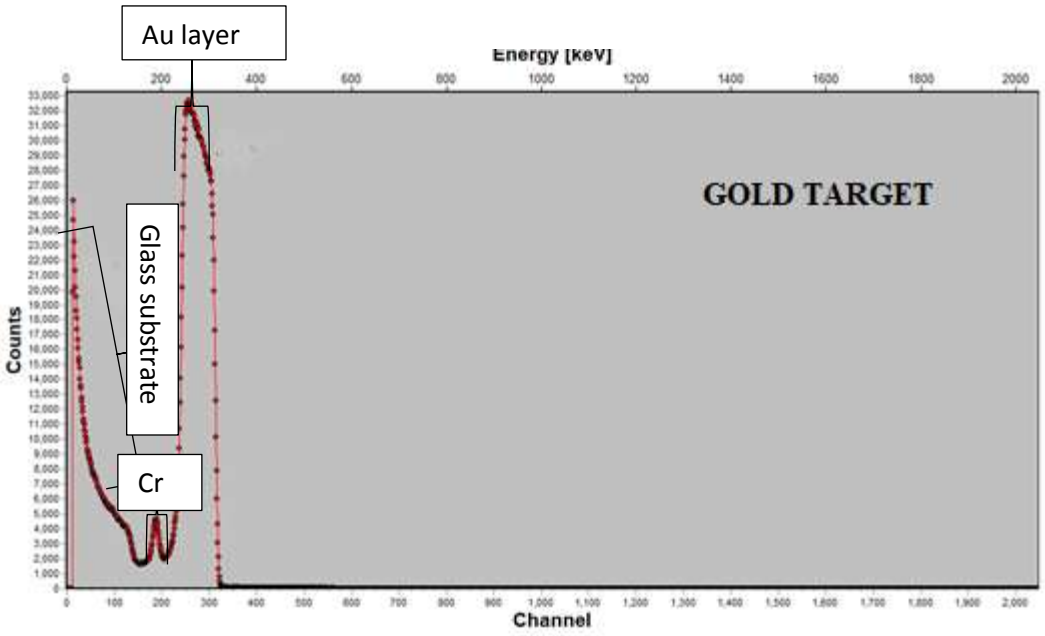

Figure 4. 15: Raw (undeconvoluted) gold spectrum at accelerator terminal voltage of 0.4 MV

The gold target is made of gold on a thick glass substrate, with a thin chromium layer sandwiched in between. In the spectrum, the layer with highest channel of detection is gold (Au) followed by the thin chromium (Cr) layer and the thick silicon (glass) substrate.

There was a greater interaction between the helium particles and the gold elements thereby producing the sharp peak immediately. The gold layer is observed to have more counts since the helium beam interacted with more particles in the gold layer.

There were more scattered peaks in the regions of the chromium and the glass substrate. This was due to less interaction between the helium particles and the chromium and the glass substrate as the energy of the helium particles had reduced after interacting with the gold layer. The less beam interaction between the chromium layer and the glass substrate contributed to the lesser peak counts observed in those layers.

The gold layer was fitted to determine its true channel of detection. The red curve represents the experimental simulation whereas the blue curve represents the calibrated simulation. This is shown in figure 4.16.

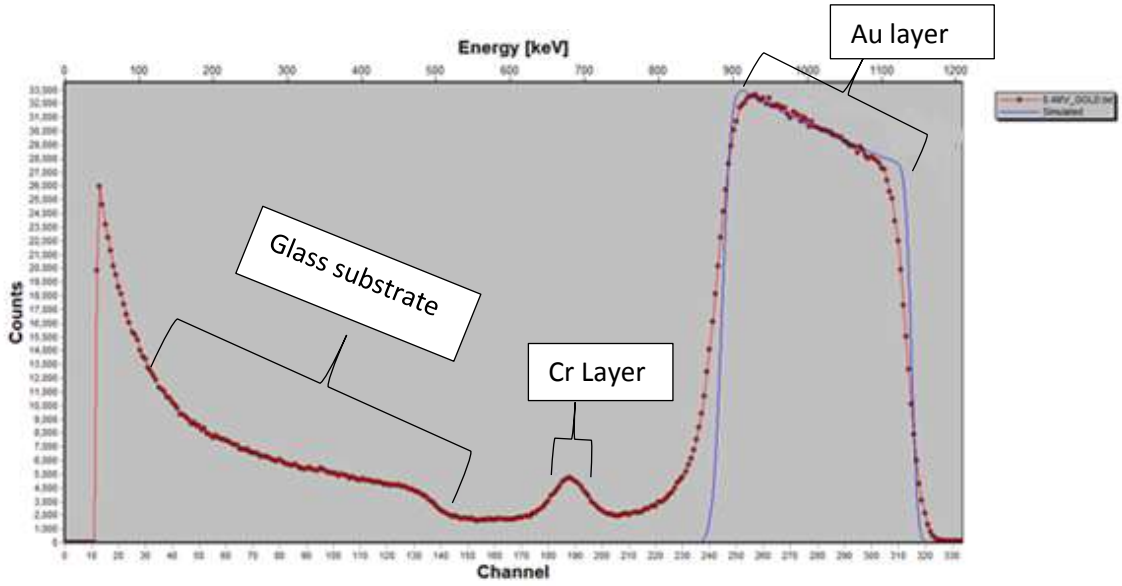

Figure 4. 16: Calibrated Gold layer at terminal accelerating voltage of 0.4 MV

In fitting the gold in figure 4.15, the particle sr and the energy per channel of the spectra were adjusted to 8.65×10^{10} particles sr and 3.62 KeV/Ch respectively for an incident helium beam of 0.4 MV.

After the fitting process, the channel for detecting the gold layer at 0.4 MV terminal accelerator voltage was subsequently found to be 308.

Figure 4.17 represents the raw (undeconvoluted) spectrum generated when helium beam accelerated at 0.7 MV interacted with the gold target.

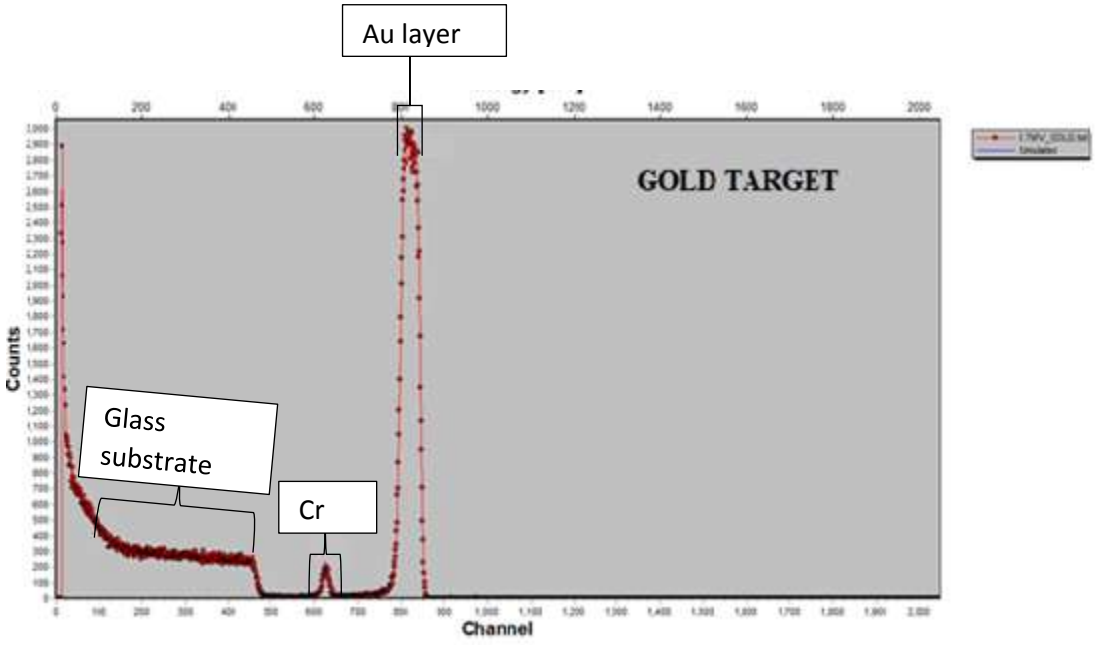

Figure 4. 17: Raw (undeconvoluted) gold spectrum at accelerator terminal voltage of 0.7 MV

The gold target is made of gold on a thick glass substrate, with a thin chromium layer sandwiched in between. In the spectrum, the element with highest channel of detection is gold (Au) followed by the thin chromium (Cr) layer and the thick silicon substrate.

There was a greater interaction between the helium particles and the gold elements thereby producing the immediate sharp peak.

More scattered peaks were found in the regions of the chromium and the glass substrate. This is as a result of less interaction between the helium particles and the chromium and the glass substrate as the energy of the helium particles reduced after interacting with the gold layer situated at the surface of the gold target. The reduced particle interaction in the chromium and the glass layers resulted in the reduced peak counts in these two regions.

The gold layer was fitted to determine its true channel of detection. The red curve represents the experimental simulation whereas the blue curve represents the calibrated simulation. This is shown in figure 4.18.

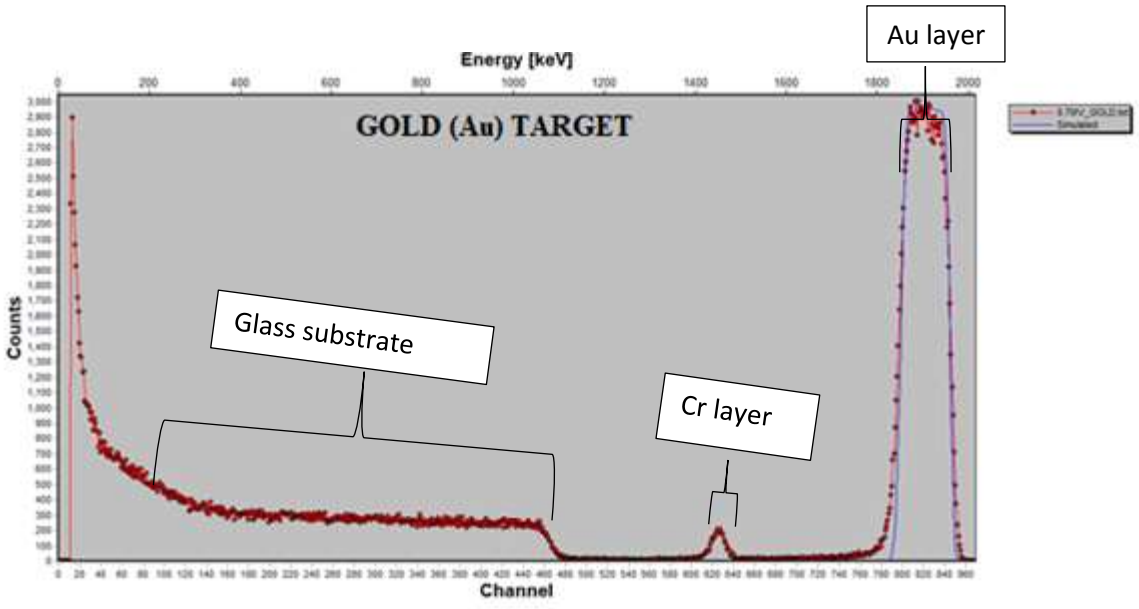

Figure 4. 18: Calibrated Gold layer at terminal accelerator voltage of 0.7 MV

In fitting the gold in figure 4.18, the particle sr and the energy per channel of the spectra were adjusted to 3.70×10^{10} particles sr and 2.32 KeV/Ch respectively for an incident helium beam of 0.7 MV.

After the fitting process, the channel for detecting the gold layer at 0.7 MV terminal accelerator voltage was found to be 820.

Figure 4.19 shows the raw (undeconvoluted) generated when helium beam accelerated at 0.9 MV interacted with the gold target.

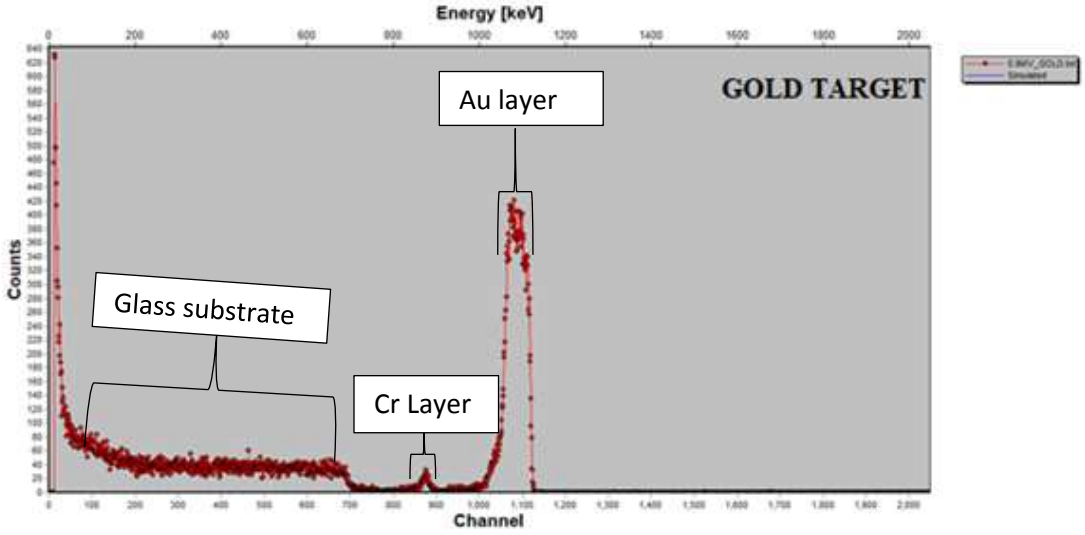

Figure 4. 19: Raw (undeconvoluted) gold spectrum at accelerator terminal voltage of 0.9 MV

Obviously, the gold target is made of gold, with a thin chromium layer sandwiched between the thick glass substrate. In the spectrum, the layer with largest channel of detection is gold (Au) followed by the thin chromium (Cr) layer and the thick silicon substrate.

There was a greater interaction between the helium particles and the gold elements thereby producing the sharp peak with the highest peak count.

There were more scattered peaks in the regions of the chromium and the glass substrate. This was due to less interaction between the helium particles and the chromium and the glass substrate as the energy of the helium particles had reduced after interacting with the gold layer. The reduced interaction in these two regions caused the reduced peak counts for the chromium layer and the glass substrate.

The gold layer was fitted to determine its true channel of detection. The red curve represents the experimental simulation whereas the blue curve represents the calibrated simulation. This is shown in figure 4.20.

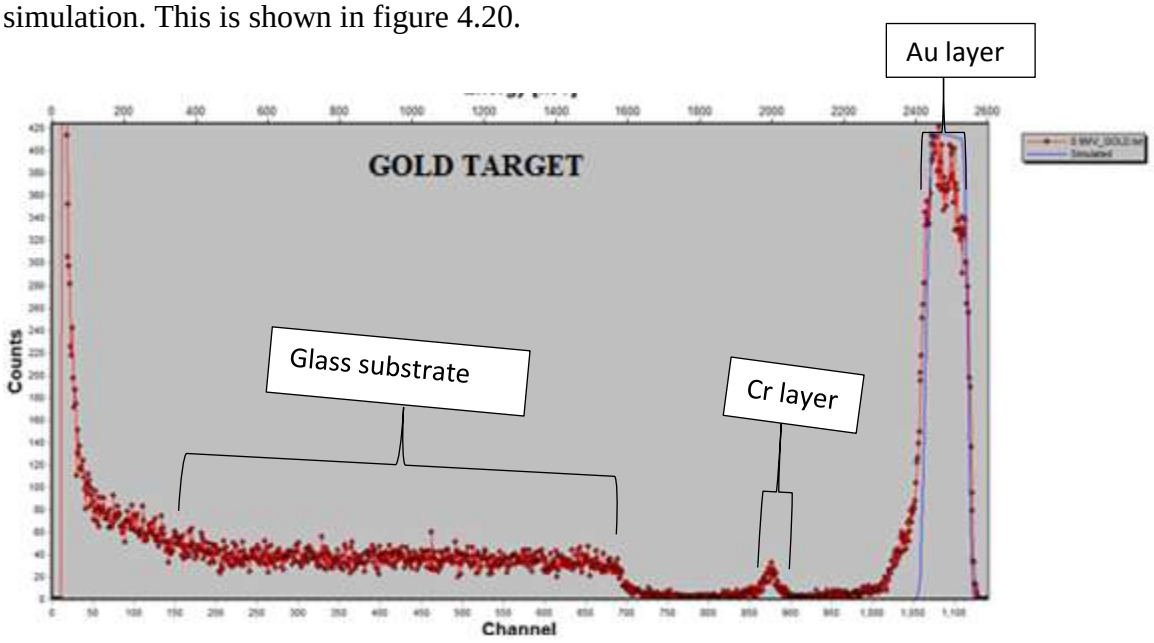

Figure 4. 20: Calibrated Gold layer at accelerator terminal voltage of 0.9 MV

In fitting the gold layer in figure 4.15, the particle sr and the energy per channel of the spectra were adjusted to 8.08×10^9 particles sr and 2.28 KeV/Ch respectively for an incident helium beam of 0.9 MV.

After the fitting process, the channel for detecting the gold layer at 0.9 MV terminal accelerator voltage was subsequently found to be 1090.

Figure 4.21 represents the raw (undeconvoluted) spectrum generated when helium beam accelerated at 1.096 MV interacted with the gold target.

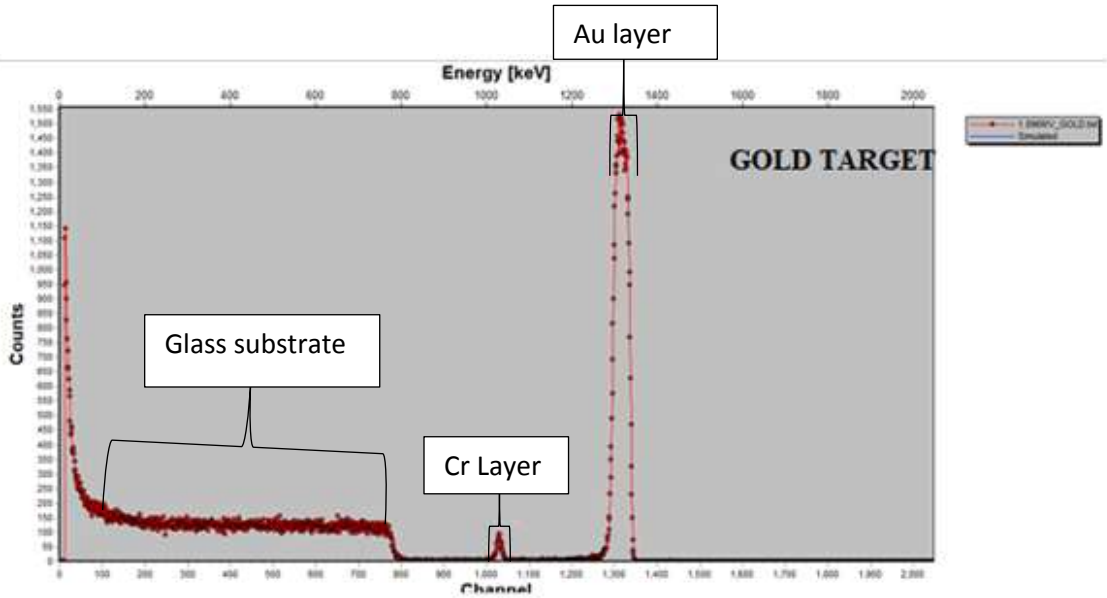

Figure 4. 21: Raw (undeconvoluted) gold spectrum at accelerator terminal voltage of 1.096 MV

The gold target is made of gold, sandwiched with a thin chromium layer sitting on a thick glass substrate. In the spectrum, the layer with highest channel of detection is gold (Au) followed by the thin chromium (Cr) layer and the thick silicon substrate.

There was a greater interaction between the helium particles and the gold elements thereby producing the sharp peak immediately.

There were more scattered peaks in the regions of the chromium and the glass substrate. This was due to less interaction between the helium particles and the chromium and the glass substrate as the energy of the helium particles had reduced after interacting with the gold layer.

The gold layer was fitted to determine its true channel of detection. The red curve represents the experimental simulation whereas the blue curve represents the calibrated simulation. This is shown in figure 4.22.

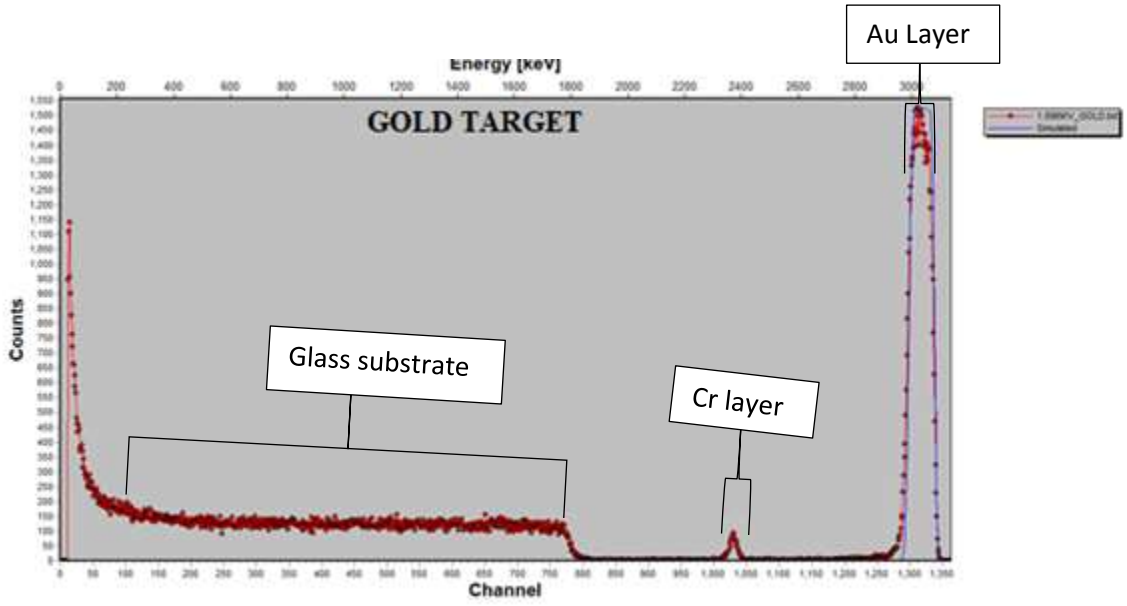

Figure 4. 22: Calibrated Gold layer at terminal accelerating voltage of 1.096 MV

In fitting the spectrum in figure 4.21, the particle sr and the energy per channel of the spectra were adjusted to 4.02×10^{10} particles sr and 2.302 KeV/Ch respectively for an incident helium beam of 1.096 MV.

After the fitting process, the channel for detecting the gold layer at 0.4 MV terminal accelerator voltage was subsequently found to be 1320.

Figure 4.23 represents the raw (undeconvoluted) spectrum generated when helium beam accelerated at 1.198 MV interacted with the gold target.

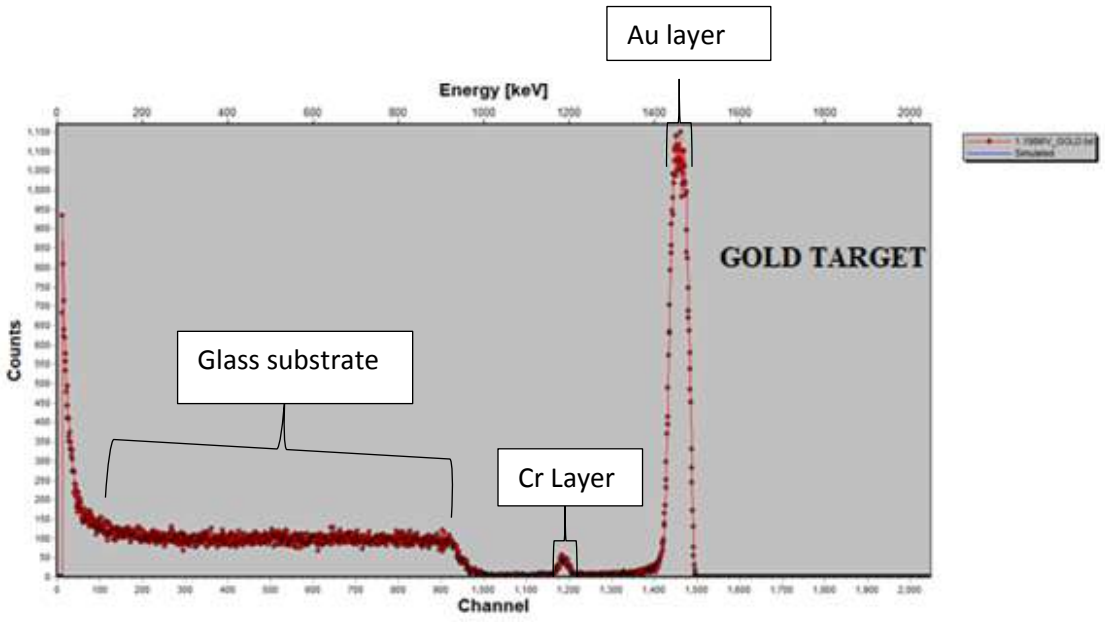

Figure 4. 23: Raw (undeconvoluted) gold spectrum at accelerator terminal voltage of 1.198 MV

The gold target is made of gold on a thick glass substrate, with a thin chromium layer sandwiched in between. In the spectrum, the layer with highest channel of detection is gold (Au) followed by the thin chromium (Cr) layer and the thick silicon substrate.

There was a greater interaction between the helium particles and the gold elements thereby producing the sharp peak immediately.

There were more scattered peaks in the regions of the chromium and the glass substrate. This was due to less interaction between the helium particles and the chromium and the glass substrate as the energy of the helium particles had reduced after interacting with the gold layer.

The gold layer was fitted to determine its true channel of detection. The red curve represents the experimental simulation whereas the blue curve represents the calibrated simulation. This is shown in figure 4.24.

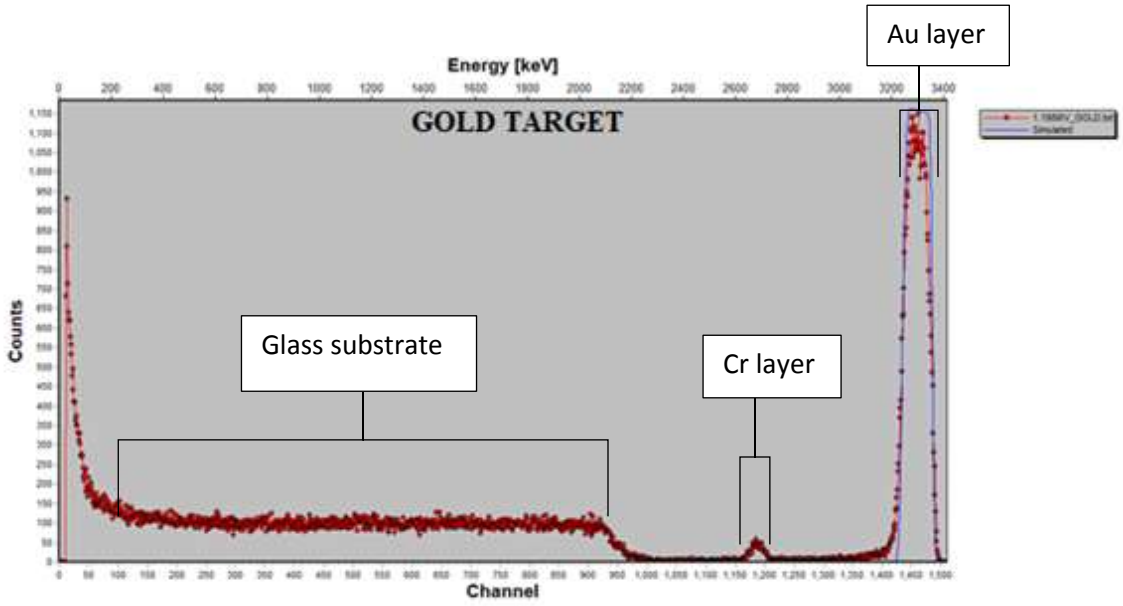

Figure 4. 24: Calibrated Gold layer at accelerator terminal voltage of 1.198 MV

In fitting the spectrum in figure 4.23, the particle sr and the energy per channel of the spectra were adjusted to 8.08×10^9 particles sr and 2.28 KeV/Ch respectively for an incident helium beam of 1.198 MV.

After the fitting process, the channel for detecting the gold layer at 1.198 MV terminal accelerator voltage was subsequently found to be 1460.

It is observed that, irradiating the gold target at the five different and increasing accelerating voltages, the channels of observing the gold layer increased as well. This is as shown in Table 4.2.

Table 4. 2: Data of gold spectra fits at five different accelerator voltages

Voltage, V_m (MV)	Particles Sr.	Energy/Channel offset (KeV/Ch)	Channel(C)
0.4	8.6×10^{10}	3.62	308
0.7	3.7×10^{10}	2.32	820
0.9	8.08×10^{9}	2.28	1090
1.096	4.02×10^{10}	2.302	1320
1.198	3.56×10^{10}	2.26	1460

The channel of detecting the gold layer increased when the incident beam energy was increased because, at a higher energy, the helium beam and gold layer interaction rate was higher causing most of the gold particles to interact quicker.

The result of a plot of channel number (C) as a function of terminal accelerator voltage (V_m) is as shown in figure 4.25. From this plot, the channels of observing the gold target is directly proportional to the accelerating voltages.

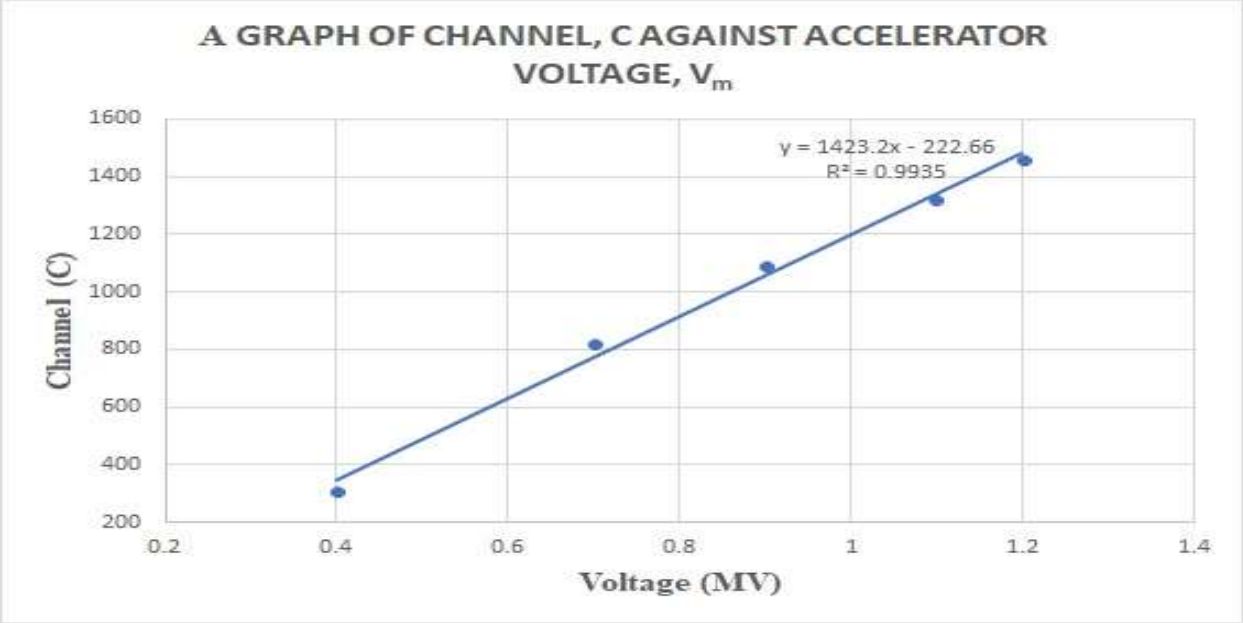

Figure 4. 25: A plot of channel (C) against accelerating voltages ($\boldsymbol{V_m}$)

From the plot, slope has been found to be 1423.2 channels and the intercept -222.66 channels.

That is, the intercept, $(C_O + nk\beta V_O) = 1423.2$ and the slope, $nk\alpha\beta = 1423.2$ channels. Using the values of n=2, k=0.9141, β=962.8 channels/MV and C_o= -70.24 channels V_o and α are calculated as;

$$V_o = \frac{Intercept - C_O}{nk\beta} = \frac{-222.66-(-70.24)}{0.9141\times962.8} = -0.173\ MV \quad (4.3)$$

$$\alpha = \frac{Slope}{nk\beta} = \frac{1423.2}{0.9141\times962.8} = 1.617\ MeV/MV \quad (4.4)$$

The α beam energy calibration equation becomes,

$$E = -0.173n + 1.617nV_m \text{ (MeV), n=2} \quad (4.5)$$

Or

$$E = -0.35 + 3.23V_m \text{ (MeV)} \quad (4.6)$$

The established experimental equation in this work is similar to the theoretical beam energy calibration equation,

$$E = nV_O + n\alpha V_m \text{ (MeV)} \quad (4.7)$$

The fits shown in fig 4.27 reveals the linear dependence of *E* on *V*, and C on *E*.

4.4 VALIDATION OF THE IMPLEMENTED CALIBRATION METHOD AND EQUATION

The general equation governing tandem acceleration of ion beams through particle accelerators is given as:

$$E = E_i + nV_{m,} \quad (4.8)$$

E_i is the injection energy of the ion, n is the charge state of the helium beams. This equation theoretically predicts the energy a charged helium ion beam would produce when accelerated by the tandem accelerator at GAEC.

Table 4.3 compares the predicted or theoretical helium beam energies at different accelerator voltages to the experimental energies (employed eqn. 4.6).

Table 4. 3: Theoretical beam energies at different accelerator voltages verses experimental beam energies

Voltage (MV)	Theoretical Energy (MeV)	Experimental energy (MeV)	Energy Difference (MeV)	Energy Difference (%)
0.4	1.237	0.942	0.295	29.5
0.7	2.124	1.911	0.213	21.3
0.9	2.758	2.557	0.201	20.1
1.096	3.338	3.19	0.148	14.8
1.198	3.637	3.52	0.117	11.7
1.2	3.649	3.526	0.123	12.3
1.3	3.951	3.849	0.102	10.2
1.4	4.253	4.172	0.081	8.1
1.5	4.555	4.495	0.06	6
1.6	4.857	4.818	0.039	3.9
1.7	5.159	5.141	0.017	1.7

It is observed in the table that, there was a decrease in the difference in energies as the accelerator voltage increased. That is, at higher operating voltages of the accelerator, the error margin in energy of ion beam produced from the accelerator system is minimal. Conversely, at lower operating terminal voltages of the accelerator system the energy error margin widens.

The theoretical and experimental energies relate with an R-squared energy of 1, indicating a strong correlation within the theoretical and experimental beam energies. Therefore, the same nuclear reactions occur in both the theoretical and experimental beam energies. This is as shown in the graph in figure 4.26.

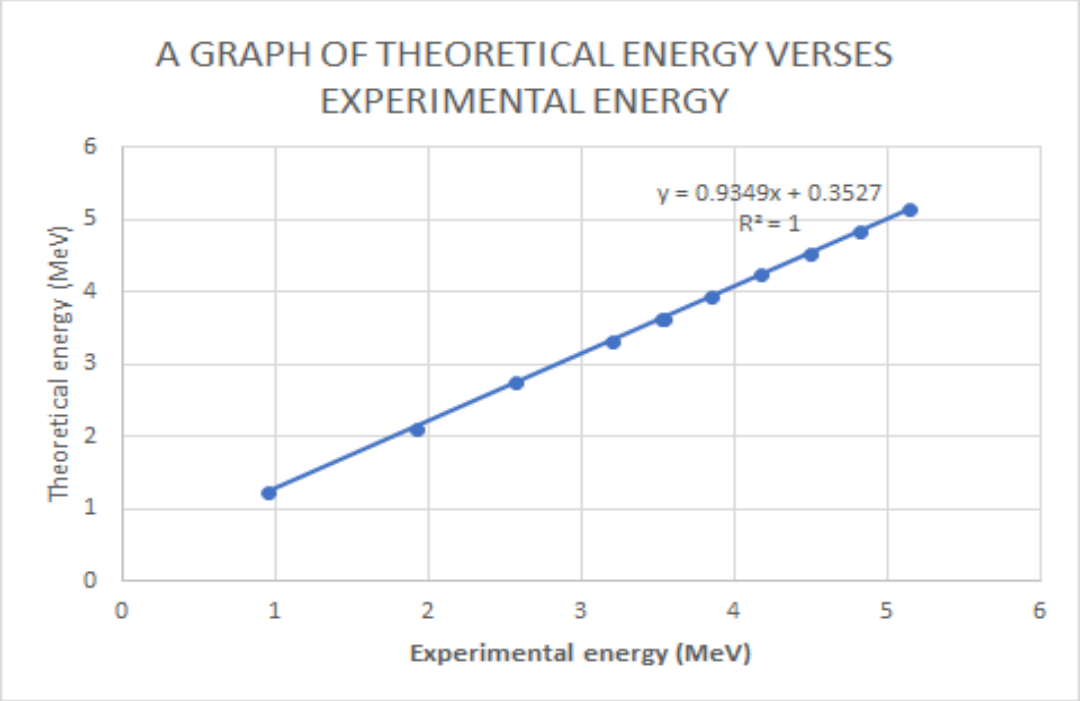

Figure 4. 26: Correlation between theoretical energy and the experimental energy at 10 different accelerator voltages

Also, the newly computed energies based on the accelerator energy calibration were tested on a 2 MeV $^{27}Al(\alpha,\alpha_0)^{28}Si$ nuclear reaction analysis of an sample containing aluminum (Al). Spectra were collected for RBS, background (RBG), PIXE, and nuclear reaction analysis (NRA) as shown in figure 4.27.

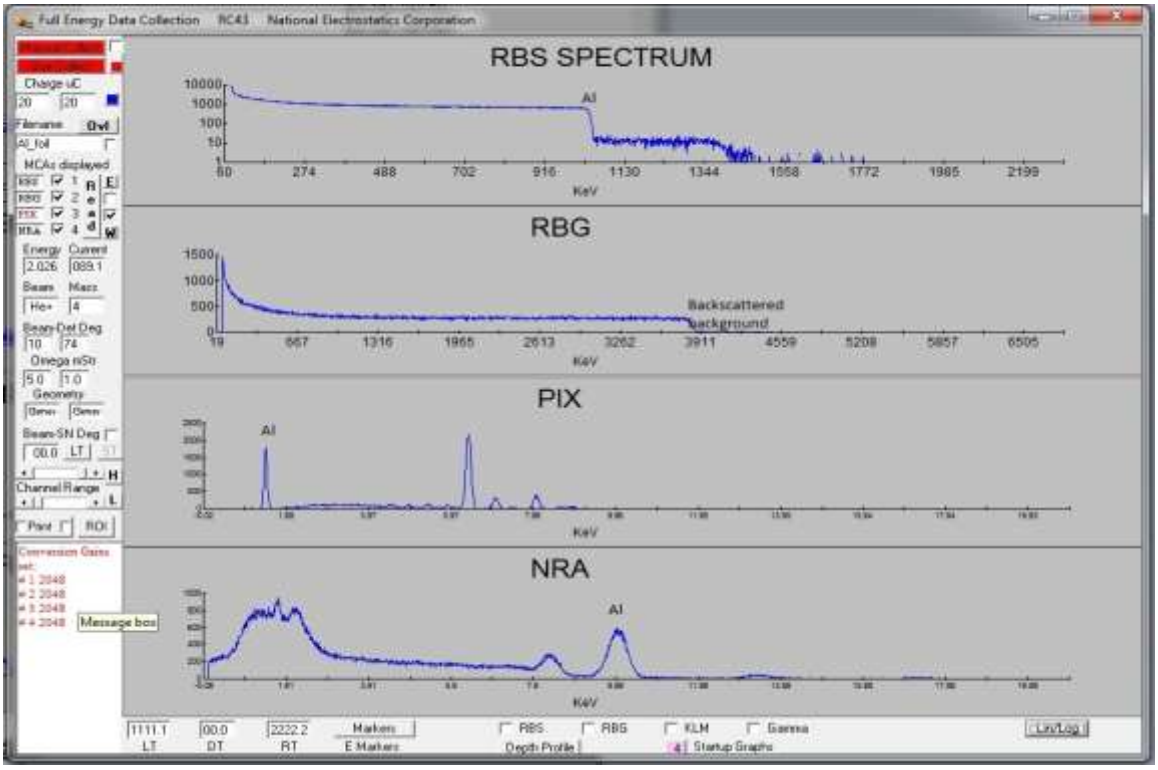

Figure 4. 27: Spectra from ion beam analysis of aluminum target using 2.026 MeV helium beam output energy

The PIXE spectrum indicates the elemental composition of the target material. In this case the element determined is aluminum (Al). The RBS spectrum indicates the thickness of the aluminum (Al) target. Also, the RBG spectrum is the background which reveals the impurities in the aluminum (Al) target.

The results show that the energy calibration was in the acceptable range since the ion beam energy output, 2.026 MeV was able to produce a low cross-section nuclear reaction such as $^{27}Al(\alpha,\alpha_0)^{28}Si$ based on comparison with published nuclear data in the International Atomic Energy Agency (IAEA) IBANDL database which made use of an ion beam energy output of 2.0 MeV. There was a deviation of 0.026 MeV (1.3%) in beam output energy to

cause the $^{27}Al(\alpha,\alpha_0)^{28}Si$ nuclear reaction. This deviation is insignificant in having any effect on the $^{27}Al(\alpha,\alpha_0)^{28}Si$ nuclear reaction.

CHAPTER 5

CONCLUSIONS AND RECOMMENDATIONS

5.1 CONCLUSIONS

The 1.7 MV tandem accelerator at the Accelerator Research Centre (ARC) of the Ghana Atomic Energy Commission (GAEC) has successfully been calibrated through the use of the Rutherford Backscattering Spectrometry (RBS) technique. The calibration procedure ensured that the energy of the accelerated helium ions from the accelerator facility were known with a high precision and accuracy.

The detector system calibration was performed with the consequent determination of the system off-set.

The accelerator system parameters (off-set in terminal voltage volt-meter reading) were accurately measured through the system calibration carried out.

This technique of ion beam energy calibration has been found to be very simple and time saving. This is because only five steps of energy ranges were used during the processes of the ion beam energy calibration as compared to the several runs of energy range used in nuclear resonance technique of ion beam energy calibration at the ARC facility.

Also, the newly adopted method of ion beam energy calibration is cost effective. This method does to require running of the accelerator to cover a wide energy range in order produce the needed nuclear reactions to perform the energy calibration. Operating the accelerator for extended runtime means one must consider the high cost involved in purchasing electricity for such operations. Also, this technique did not require any complex

instrumentation or that any change be made to the existing experimental setup at the ARC facility of GAEC being utilized for ion beam analysis (IBA).

Helium ion beam energy calibration using the new method is achieved within a shorter time as compared to the nuclear resonance method of ion beam energy calibration. The current method has proved reduced accelerator run-time and less man-hour (labour) usage.

A model beam energy calibration for the ARC facility has been established as:

$$\mathbf{E = -0.35n + 3.23V_m} \text{ (MeV)} \qquad (5.1)$$

This experimentally determined helium beam energy calibration equation agrees with the theoretical tandem ion beam energy accelerator equation. The new energies derived from the calibration procedure were tested with the alpha particle – aluminum nuclear reaction $^{27}\mathrm{Al}(\alpha, \alpha_o)^{27}$. This result was found to be in good agreement with published Al nuclear reaction resonance data in the IAEA IBANDL database (https://www-nds.iaea.org/exfor/ibandl.htm).

This simple, time saving, cost effective and efficient RBS technique of ion beam energy calibration technique has successfully been adopted and implemented at the ARC facility.

5.2 RECOMMENDATIONS

In view of the various methods of calibrating helium ion beams of particle accelerators;

- It is recommended that ARC facility use this current method of energy calibration alongside the existing method for a longer period and conduct full-scale comparison.
- Particle accelerator centres could also employ the RBS technique to routinely calibrate their accelerators as this method is simple, time saving, efficient and cost effective.
- It is recommended that future works be directed to calibrating the proton beam lines using the RBS technique.

REFERENCES

Accelerator Systems. National Electrostatic Corporation (NEC). https://www. pelletron.com. [Retrieved on March 3, 2018]

Bachiller-Perea, D., Munoz-Martin, A., Corvisiero, P., Jimenez-Rey, D., Joco, V., Maira and Zucchiatti, A. (2013). New energy calibration of the CMAM 5MV tandem accelerator. Energy Proceedings,4, pp. 57–63. https://doi.org/10.1016/j.egypro.2013.09.007

Barbalat, O. (1994). Applications of particle accelerators. Prepared for the International Committee for Future Accelerators (ICFA) Panel on Spin-Off from Particle Physics. 34(6), pp. 841–853.

Bichscl, H. (1965). Procedia International Symposium on Magnet technology.Stanford University, Stanford, California.pp. 467.

Brindhaban, S.A., Barker, P.H., Keeling, M.J and Wood, W.B. (1994). Accelerator Beam Energy Calibration with the ^{27}Al(p, n) and ^{27}Al(p,γ) Reactions. Nuclear Instruments and Methods in Physics Research Section A: Accelerators, Spectrometers, Detectors and Associated Equipment. 340,pp. 436-441.

Bryant, P.J. (1994). A brief history and review of accelerators. European Organization for Nuclear Research. pp. 1-4. http://spazioinwind.libero.it/maioli/data/fsa5.pdf

Camas, J.,Crockford, G., Ferioli, G., Fischer C.,Gras, J.J., Jung, R., Koopman, J., and Mann, J.(1993). High Resolution Measurements of Lepton Beam Transverse Distributions with the LEP Wire Scanners. Proceedings on International Conference of Particle Accelerators.4, pp. 2649-2651. doi: 10.1109/PAC.1993.309370

Cheng, H.S., Shen, H., Yang, F. and Tang, J. (1994). IBANDL database. Nuclear Instruments and Methods in Physics. B85, pp.47. https://www-nds.iaea.org/exfor/ibandl.htm. [Retrieved on July 25, 2018]

Chu, W.K., Mayer, J.W., and Nicolet, M.A., (1978). Backscattering Spectrometry. pp. 384.Academic press, New York, U.S.A. http://garfield.library.upenn.edu/classics1980/A1980KD94100001.pdf.

Cockroft,J.D. and Walton, E. T. S. (1932). Experiments with High Velocity Positive Ions.Proceedings of the Royal Society.A136, pp. 619–630. http://dx.doi.org/10.1098/rspa.1932.0107.

Colaux, J. L., Terwagne, G., and Jeynes, C. (2015). On the traceably accurate voltage calibration of electrostatic accelerators. Nuclear Instruments and Methods in Physics Research, Section B: Beam Interactions with Materials and Atoms, 349, pp. 173–183. https://doi.org/10.1016/j.nimb.2015.02.048

Courant, E.D., Livingston, M.S., and Snyder H.S (1952). The Strong Focusing Synchroton-A New High- Energy accelerator.American Physical Society. 88(5),pp. 1-4. https://doi.org/10.1103/PhysRev.88.1190.

GAEC. (2015). Annual report of the National Nuclear Research Institute(NNRI),Ghana Atomic Energy Commission, pp.4-8.

Glass, G. A., Mcdaniel, F., Doyle, B. L., Duggan, J. L., Galindo-Uribarri, A., Hayes-Sterbenz, A., and Schulte, R. (2014). 23rd International Conference on the Application of Accelerators in Research and Industry,Caari.5, pp. 32-33.

Goldberg, D.A and Lambert, G.R.(1992). Dynamic Devices.A Primer on Pickups and

Kickers. In AIP Conference Proceedings.249(1), pp. 9–10. https://doi.org/10.1063/1.41979

Gross, E. E.(1976). Calibration of an analyzing magnet using an alpha source. Nuclear Instruments and Methods. 135, pp. 401–402. https://doi.org/10.1016/0029-554X(76)90191-9

Gurbich, A.F (1998). Evaluation of Non-Rutherford Proton Elastic Cross-Section For Carbon. Nuclear Instruments and Methods in Physics Research.136-138, pp. 60-65. https://doi.org/10.1016/S0168-583X(97)00837-9

Healy, M. J. F. (2006). Energy calibration by silicon resonance: Completing system calibration with one reference material. Nuclear Instruments and Methods in Physics Research, Section B: Beam Interactions with Materials and Atoms, 249, pp. 918–920. https://doi.org/10.1016/j.nimb.2006.03.163

Kelly, R. (2000). Calibration of a 1.7 MV Pelletron Accelerator. pp. 1-10. University of Florida, Florida,USA.

Kerst, D. W. (1941). The Acceleration of Electrons by Magnetic Induction. Physical Reviews Journal. 60, pp. 47. https://doi.org/10.1103/PhysRev.60.47

Knoll, G. (2000). Radiation dectection and measurement. 2,pp. 47-48.John Willey and Sons.New York,USA.

Koziol, H. (1992). Beam diagnostics for accelerators. European Organization for Nuclear Research .1,pp. 5-7.

Kureba, C. O. (2010). Energy calibration of the 6 MV EN Tandem Accelerator of iThemba Labs (Gauteng) and Measurement of ^{16}O + ^{16}O elastic scattering. pp. 70.

http://mobile.wiredspace.wits.ac.za/bitstream/handle/10539/9247/KUREBAMScRR.pdf?sequence=1

Lane, D.W., Avery, A.J.,Parttridge, G., and Healy, M. (1993). A simple accelerator calibration procedure. Nuclear Instruments and Methods in Physics Research. 73(370-332), pp. 583–586.

Lawrence,O.E. and Livingston, S.M.(1932). The Production of High Speed Light Ions Without the Use of High Voltages.Physical Reviews Journal. 40,pp. 70-74. https://doi.org/10.1103/PhysRev.40.19

Marion J.B. (1966). Accelerator Calibration Energies. In: Reviews of Modern Physics.38, pp. 660. https://doi.org/10.1103/RevModPhys.38.660.

Martin, B., Mihaelsen, R., Sethi, R.C., and Zigler, K.,(1985). A Method for the energy Calibrtion of a Heavy Ion Accelerator. Nuclear Instruments and Methods in Physics Research. A238 (1),pp.1-4. https://doi.org/10.1016/0168-9002(85)91020-4.

McMillan, E.M. (1945) The synchrotron - A Proposed High-Energy Particle Accelerator. Physical Reviews Journal.68,pp. 143. https://doi.org/10.1103/PhysRev.68.143.

Oura, K.; Lifshits, V.G.; Saranin, A.A.; Zotov, A.V and Kayam, M. (2003). In Surface Science: An Introduction. Springer. Berlin,Germany.

Olsen, D.K.,Erb, K A.,Jones C. M., Milner W.T., Weisser D.C., and Ziegler N.F.(1987). Calibration of the HHIRF Tandem Accelerator Energy Analyzing Magnet. Nuclear Instruments and Methods in Physics Research. A254, pp. 1-6.

Pollock, T. J. (2015). Operations Manual for the NEC RC43 Analytical Software for the Ghana Endstation. National Electrostatics Coorporation. 5.2,pp.16-22.

M. M. Abdel Rahman, M.M.A.(2012). Ion Sources for Use in Research and Low Energy Accelerators. International Journal of Instrumentation Science. 1(5), pp. 63-77. doi:10.5923/j.instrument.20120105.02.

Roxana, C., Pantelica, D., Cata-Dahl,G.,Petrascu,H.,Velisa,G.,Ionescu, P., Ghita G.D.,Filipescu, M.(2012). The Energy Calibration of The Bucharest FN Tandem Accelerator. U.P.B Science Bulletin. A:74,pp. 2-3.

Sarah, W. (2017). Ten things you might not know about particle accelerators. The Symmetry Magazine Database. https://www.symmetrymagazine.org/article.

[Retrieved on January 1,2018]

Scott, H.L and Lusby, T.F. (1975). Iintensity Measurements of the y-ray decay Of ^{27}Si via the ^{27}Al(p,γ)^{27}Si Ep = 992 keV Resonance, 31(Li), 517–520. Nuclear Instruments and Methods in Physics Research.131, pp. 517-520.

Scott D and Paine B. (1983). Accelerator energy calibration using non-resonant nuclear reactions. Nuclear Instruments and Methods in Physics Research. 218, pp. 154- 158.

Shamu R.E.;Bernstein E.M.;M.J.Parrot. (1974). Accelerator Energy Calibration Using the ^{12}C(α,n$_o$)^{15}O . Nuclear Instruments and Methods in Physics Research. 114, pp. 605–608. https://doi.org/10.1016/0029-554X(74)90187-6.

Tesmer, J.R and Nastasi. (1995). Handbook of Modern Ion Beam Materials Analysis.Materials Research Society.11,pp.33-37.

Uhrmacher M., Pampus K., Bergmeister F.J.,Purschke D., Lieb, K.P.(1985). Energy Calibration of the 500 kV Heavy Ion Implanter IONAS. Nuclear Instruments and Methods in Physics Research. B9, pp. 234-242. https://doi.org/10.1016/0168-

583X(85)90688-3

Van De Graaff, J.R. (1931). A 1,5000,000 volt electrostatic generator.Proceeding of the American Physical Society. 38(1919), pp. 1-2.15. http://web.ihep.su/dbserv/compas/src/van%20de%20graaff31/eng.pdf

What is Calibration and Why is it Important? https://www.tempcon.uk.com. [Retrieved on April 17,2018]

Widerøe, R. (1928). About a new principle for the production of high voltages .Arch. Elektrotech. 21(4),pp. 387-406.